



# Reconstructing past variations in environmental conditions and paleoproductivity over the last ~ 8000 years off north-central Chile (30° S)

Práxedes Muñoz<sup>1,2</sup>, Lorena Rebolledo<sup>3,4</sup>, Laurent Dezileau<sup>5</sup>, Antonio Maldonado<sup>2,6</sup>, Christoph Mayr<sup>7,8</sup>, Paola Cárdenas<sup>4</sup>, Carina B. Lange<sup>4,10,11</sup>, Katherine Lalangui<sup>9</sup>, Gloria Sanchez<sup>12</sup>, Marco Salamanca<sup>10</sup>, Karen Araya<sup>1,13</sup>, Ignacio Jara<sup>2</sup>, Gabriel Easton<sup>14</sup>, and Marcel Ramos<sup>1,2</sup>

<sup>1</sup>Departamento de Biología Marina, Universidad Católica del Norte, Larrondo 1281, Coquimbo, Chile

<sup>2</sup>Centro de Estudios Avanzados en Zonas Áridas (CEAZA), La Serena, Coquimbo, Chile

<sup>3</sup>Departamento Científico, Instituto Antártico Chileno, Punta Arenas, Chile

<sup>4</sup>Centro FONDAP de Investigación Dinámica de Ecosistemas Marinos de Altas Latitudes (IDEAL), Universidad Austral de Chile, Campus Isla Teja, Valdivia, Chile

<sup>5</sup>Normandy University, UNICAEN, UNIROUEN, CNRS, M2C, 14000 Caen, France

<sup>6</sup>Instituto de Investigación Multidisciplinario en Ciencia y Tecnología, Universidad de La Serena, La Serena, Chile

<sup>7</sup>Institut für Geographie, FAU Erlangen-Nürnberg, 91058 Erlangen, Germany

<sup>8</sup>Department of Earth and Environmental Sciences and GeoBio-Center, LMU Munich, 80333 Munich, Germany

<sup>9</sup>Planta de Alimentos Pargua, AquaChile, Puerto Montt, Chile

<sup>10</sup>Departamento de Oceanografía, Facultad de Ciencias Naturales y Oceanográficas, Universidad de Concepción, Casilla 160C, Concepción, Chile

<sup>11</sup>Centro de Investigación Oceanográfica COPAS Sur-Austral, Universidad de Concepción, Casilla 160C, Concepción, Chile

<sup>12</sup>Departamento de Ciencias y Recursos Naturales, Universidad de Magallanes, Punta Arenas, Chile

<sup>13</sup>Laboratoire Géosciences Montpellier (GM), Université de Montpellier, 34095 Montpellier CEDEX 05, France

<sup>14</sup>Departamento de Geología, Universidad de Chile, Santiago, Chile

**Correspondence:** Práxedes Muñoz (praxedes@ucn.cl)

Received: 4 September 2018 – Discussion started: 11 September 2018

Revised: 4 August 2020 – Accepted: 19 August 2020 – Published: 24 November 2020

**Abstract.** The aim of this project was to establish past variations in the main oceanographic and climatic features of a transitional semiarid ecosystem on the north-central Chilean coast. We analyzed recent sedimentary records retrieved from two bays, Guanaqueros and Tongoy (30° S), for geochemical and biological analyses, including the following: sensitive redox trace elements, biogenic opal, total organic carbon (TOC), diatoms and stable isotopes of organic carbon and nitrogen. Three remarkable periods were established with different environmental conditions and productivities: (1) > 6600 cal BP, (2) 4500–1800 cal BP and (3) 140 cal BP to the present (2015 CE). The first period was characterized by a remarkably higher productivity (higher diatom abundances and opal) in which large fluxes of organic compounds were also inferred from the accumulation of elements, such

as Ba, Ca, Ni, Cd and P, in the sediments. Meanwhile, significantly reduced conditions at the bottom of the bays were suggested based on the large accumulation of Mo, Re and U, showing a peak at 6600 cal BP, when sulfidic conditions could have been present. According to the pollen moisture index (PMI), this was also identified as the driest interval. These conditions should be associated with an intensification of the Southern Pacific Subtropical Anticyclone (SPSA) and stronger southerly western winds, emulating La Niña-like conditions, as has been described for the SE Pacific during the early Holocene and part of the mid-Holocene. During most of the second period, lower productivity was observed; however, a small increase was identified between 3400 and 4000 cal BP, although lower amounts of diatom (valves g<sup>-1</sup>) and nutrient-type metal accumulations were evident. Anoxic

conditions at the bottom of the bays changed to an almost stable suboxic condition during this time interval. The third period was marked by intense oxygenation after 1800 cal BP, as observed by a drastic change in the accumulation of U, Mo and Re. This was followed by a return to more reduced conditions over the past 2 centuries, characterized by a small productivity rise after  $\sim 140$  cal BP, as suggested by the opal accumulations. Overall, lower primary productivity, lower reduced conditions at the bottom and higher-humidity conditions were established after 6600 cal BP to the present. We suggest that the oxygenation might be associated with a weak effect from the oxygen minimum zone over the shelf and intensified El Niño activity, introducing oxygenated waters to the coastal zones through the propagation of equatorial waves and establishment of conditions that reduced the primary productivity from the mid-Holocene toward the beginning of the modern era.

## 1 Introduction

The mean climatic conditions in the SE Pacific are modulated by the dynamics of the Southern Pacific Subtropical Anticyclone (SPSA) and the Humboldt Current System. The coastal-wind pattern produced alongshore varies along the SE Pacific, showing lower seasonality between 18 and 30° S and producing semipermanent upwelling (Pizarro et al., 1994; Figueroa and Moffat, 2000). This system is highly affected by the interannual variability imposed by the El Niño–Southern Oscillation (ENSO), impacting the wind intensity and therefore the productivity (Ruttlant and Fuenzalida, 1991; Blanco et al., 2002). Other climate patterns demonstrate impacts at longer timescales (interannual, decadal, interdecadal), such as the Pacific Decadal Oscillation (PDO) and the Southern Annular Mode (SAM). These patterns modify the strength and position of the southerly western winds (SWWs), producing cold (warm) periods that affect mainly winter precipitation during the positive (negative) trends of the SAM and lead to intense (weak) upwelling (Quintana and Aceituno, 2012; Ancapichún and Garcés-Vargas, 2015). In addition, the orbitally induced variations in the austral insolation influences the extent of the Antarctic sea ice and the Hadley cell, which act as important forces in the latitudinal displacement of the Intertropical Convergence Zone (ITCZ; Kaiser et al., 2008, and references therein). These fluctuations produce humid and arid conditions along the SE Pacific, where the intensity of the wind remains the key factor in the upwelling strength and therefore the supply of nutrients to the photic zone, all of which are required for the development of the primary productivity.

Off Coquimbo (30° S), there is normally semipermanent and intense upwelling forced by local winds, strongly influenced by topographic features (Figueroa and Moffat, 2000) and ENSO variability (Shaffer et al., 1999; Escribano et al.,

2004). During El Niño, the intensities of the mean winds alongshore are reduced (and vice versa during La Niña; Rahn and Garreaud, 2013), impacting the upper circulation of the ocean and affecting the oxygenation of the water column and strength of the upwelling. The high productivity that takes place close to the coast during normal periods (Escribano et al., 2004, and references therein) maintains a zone of low dissolved-oxygen content, reinforcing the oxygen minimum zone (OMZ; Helly and Levin, 2004; Ulloa et al., 2012); however, the opposite occurs during El Niño, in which oxygenated waters enter the coastal zone provided by the narrow continental shelf (Helly and Levin, 2004). This changes the normal suboxic conditions at the bottom, normal composition of macrofauna and related geochemical characteristics of the sediments, with implications that persist for several years after the event (Gutiérrez et al., 2006; Sellanes et al., 2007).

These changes in primary productivity and oxygenation at the bottom can be observed in the sedimentary records that respond to the amount of organic carbon that has settled on the surface sediments under different oceanographic and climatic conditions. The diagenetic reactions during organic-matter remineralization produce the enrichment or depletion of trace elements, which reflects the amount of settled organic matter but also reinforces the low-oxygen conditions imposed by the OMZ, all of which promotes the enrichment or depletion of trace elements (Tribovillard, 2006). Their variability in sedimentary records has been extensively used to establish temporary changes in primary productivity and changes in the oxygenation at the bottom (Nameroff et al., 2002; Zheng et al., 2002; McManus et al., 2006; Siebert et al., 2003).

North-central Chile is a semiarid zone that does not receive large fluvial contributions, except during abnormal periods such as in El Niño years, during which higher runoff has been recorded in austral winter (Valle-Levinson et al., 2000; Montecinos and Aceituno, 2003; Garreaud et al., 2009). Under this scenario, marine sediments are often highly influenced by primary production in the water column and terrestrial runoff; therefore, sedimentary records can reveal the past variability in primary production and oceanographic conditions over the shelf, which ultimately respond to the major atmospheric patterns in the region. We considered that redox trace elements off Coquimbo (30° S) respond to changes in the local hypoxia (U, Mo and Re); in addition, the nutrient-type elements are assumed to have followed the organic flux variability of the sediments (Ba, Ni and Cu), according to the interannual and interdecadal variability described for the climatic and oceanographic settings in the region. Similarly, we measured Ca, K and Pb to assess the terrigenous inputs from runoff and eolian transportation, which is also impacted by Fe and Mn (Calvert and Pedersen, 2007). Ca accumulation depends, in turn, on carbonate productivity and dissolution and has also been used as a paleoproductivity proxy (Paytan, 2009; Govin et al., 2012). We determined the enrichment and

depletion of elements to establish the primary prevailing environmental conditions during the sedimentation of particulate matter (Böning et al., 2009). In addition, we considered the diatom assemblages with biogenic opal as a measurement of siliceous export production, total organic carbon (TOC) and stable isotopes to identify variations in the organic fluxes to the bottom. Moreover, pollen grains were used to identify environmental conditions based on the climate relationship of the main vegetation formations in north-central Chile. Based on our records we were able to identify wet and dry intervals; periods with high and low organic fluxes to the sediments, which are related to changes in primary production; and changes in the redox conditions at the bottom, which in turn have been associated with the main climatic conditions described for the Holocene in this region.

## 2 Study area

The Coquimbo area (29–30° S), in the southern limit of the north-central Chilean continental margin, constitutes a border area between the most arid zones of northern Chile (Atacama Desert) and the more mesic Mediterranean climate in central Chile (Montecinos et al., 2016). Here, the shelf is narrow, and several small bays trace the coast line.

The Tongoy and Guanaqueros bays are located on the southern edge of a broad embayment between small islands to the north (29° S; Choros, Damas and Chañaral) and Lengua de Vaca Point to the south (30° S; Fig. 1), protected from southerly winds that are predominant in the region. Tongoy Bay is a narrow marine basin (10 km at its maximum width) with a maximum depth of approximately 100 m. To the northeast lies Guanaqueros Bay, a smaller and shallower basin. High-wind events are evenly distributed throughout the year and promote an important upwelling center at Lengua de Vaca Point, resulting in the accumulation of high biomass along a narrow coastal area (Moraga-Opazo et al., 2011; Rahn and Garreaud, 2013) that reaches concentrations of approximately  $20 \text{ mg m}^{-3}$  (Torres and Ampuero, 2009). In the shallow waters of Tongoy Bay, the high primary productivity results in high TOC in the water column, allowing for the deposition of fine material to the bottom; TOC rises concurrently with periods of low oxygen (Fig. 2; Muñoz et al., 2012, unpublished data). Recent oceanographic studies indicate that low dissolved-oxygen water intrusions from the shelf (Fig. 3) seem to be related to lower sea levels, resulting from annual local wind cycles at a regional mesoscale (Gallardo et al., 2017). Oceanographic time series indicate that transition times develop in short periods due to changes in the direction and intensity of the winds along the coast, with strong seasonality (<http://www.cdom.cl/estaciones.php?seccion=Oceano&estacion=BTG>, last access: 5 November 2020). The spatial and temporal variability of these processes is still under study. In addition, oceanic variability along the western coast of South Amer-

ica is influenced by equatorial Kelvin waves on a variety of timescales, from intraseasonal (Shaffer et al., 1997) and seasonal (Pizarro et al., 2002; Ramos et al., 2006) to interannual (Pizarro et al., 2002; Ramos et al., 2008).

Sedimentological studies are scarce with regard to the north-central shelf of Chile. A few technical reports indicate that sediments between 27 and 30° S are composed of very fine sand and silt with relatively low organic-carbon content (<3 % and ~5 %), except in very limited coastal areas where organic material accounts for approximately 16 % of the total material (Melo et al., 2007). Coastal weathering is the main source of continental input owing to scarce river flows and little rainfall in the zone ( $0.5\text{--}80 \text{ mm yr}^{-1}$ ; Montecinos et al., 2016; Fig. 1). Freshwater discharges are represented by creeks, which receive the drainage of the coastal range forming wetland areas in the coast and even small estuaries, such as Pachingo, located south of Tongoy (Fig. 1). These basins cover ~300 and 487 km<sup>2</sup>, respectively. The water volume in the estuaries is maintained by the influx of seawater mixed with the groundwater supply. Normally, a surface flux to the sea is observed. Freshwater discharges only occur through dry creeks that drain water during high-rainfall periods in the coastal zone (Niemeyer, 2018).

## 3 Materials and methods

### 3.1 Sampling

Sediment cores were retrieved from two bays in the Coquimbo region – Bahía Guanaqueros (core BGGC5; 30°09' S, 71°26' W; 89 m water depth) and Bahía Tongoy (core BTGC8; 30°14' S, 71°36' W; 85 m water depth; Fig. 1) – using a gravity corer (KC-Denmark) in May 2015 on board the R/V *Stella Maris II*, owned by the Universidad Católica del Norte. The length of the cores was 126 cm for BGGC5 and 98 cm for BTGC8.

Subsequently, the cores were sliced into 1 cm sections, and subsamples were separated for grain size measurements and determination of magnetic susceptibility, trace element and biogenic opal concentrations, C and N stable-isotope signatures ( $\delta^{13}\text{C}$ ,  $\delta^{15}\text{N}$ ), and TOC content. The samples first were kept frozen ( $-20 \text{ }^\circ\text{C}$ ) and then freeze-dried before laboratory analyses.

### 3.2 Geochronology ( $^{210}\text{Pb}$ and $^{14}\text{C}$ )

A geochronology was established, combining ages estimated from  $^{210}\text{Pb}_{\text{xs}}$  activities suitable for the last 200 years and radiocarbon measurements at selected depths for older ages. The quantification of  $^{210}\text{Pb}$  activities was performed through the alpha spectrometry of its daughter  $^{210}\text{Po}$  following the procedure of Flynn (1968). The (unsupported) activities of  $^{210}\text{Pb}_{\text{xs}}$  were determined as the difference between the  $^{210}\text{Pb}$  and  $^{226}\text{Ra}$  activities measured in some intervals of the sediment column. Meanwhile,  $^{226}\text{Ra}$  was measured by gamma

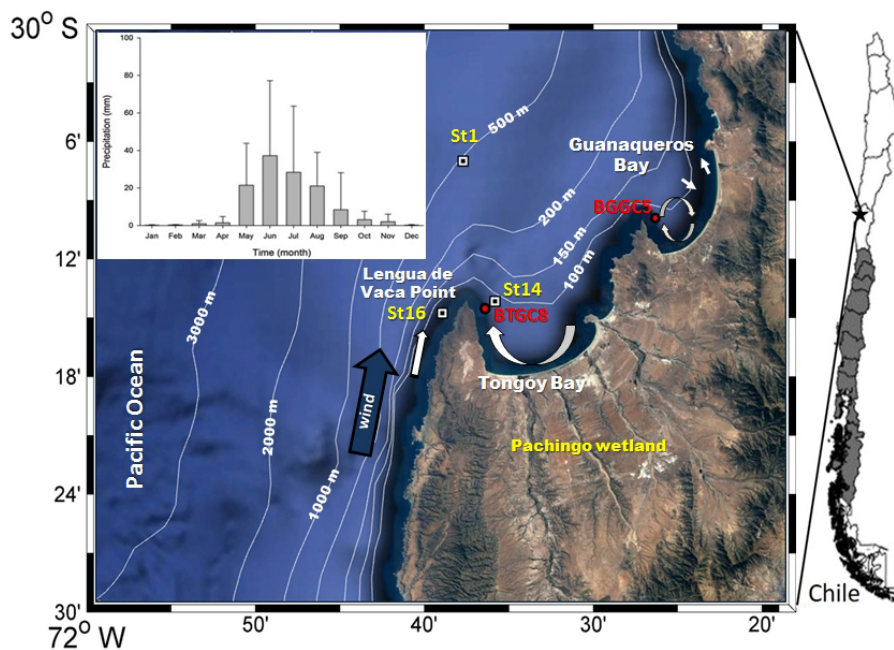


**Figure 1.** Study area showing the positions of sampling stations. Sediment cores were retrieved from Guanaqueros Bay (BGGC5) and Tongoy Bay (BTGC8) at water depths of 89 and 85 m, respectively. Information of dissolved oxygen in the water column at St1 and St16 and that of suspended organic particles collected at St14 sampling sites were gathered in a previous project (INNOVA 07CN13 IXM-150). Monthly precipitation in millimeters (bars; mean  $\pm$  SD; Montecinos et al., 2016). Schematic representation of the circulation in the bays (white arrows) and wind direction (blue arrow) is indicated, as obtained from Valle-Levinson and Moraga-Opazo (2006) and Moraga-Opazo et al. (2011).

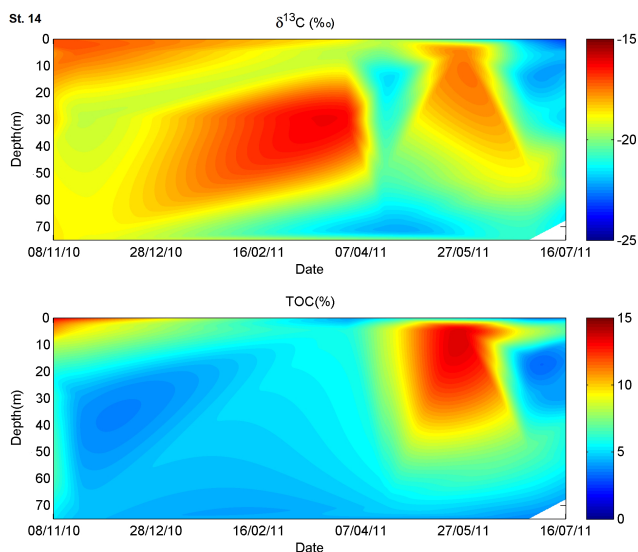


**Figure 2.** Suspended-particulate-matter composition (TOC % and  $\delta^{13}C_{org}$ ) measured in the water column between October 2010 and October 2011 at station St14, Tongoy Bay, Coquimbo (30° S).

spectrometry at the Laboratoire Géosciences of the Université de Montpellier (France). Standard deviations (SDs) of the  $^{210}Pb$  inventories were estimated by propagation of the counting uncertainties (Bevington and Robinson, 1992; Table S1 in the Supplement). The ages were based on the constant rate of supply (CRS) model (Appleby and Oldfield, 1978).

Radiocarbon measurements were performed on a mix of planktonic foraminifer species in core BGGC5, whereas the benthic foraminifer species *Bolivina plicata* was selected for core BTGC8 (Table 1). The samples were submitted to the National Ocean Sciences AMS Facility (NOSAMS) of the Woods Hole Oceanographic Institution (WHOI). The timescale was obtained from  $^{210}Pb_{xs}$  and  $^{14}C$  measurements and from Bacon age–depth-modeling open-source software (Blaauw and Christen, 2011) considering the Marine curve  $^{13}C$  (Reimer et al., 2013; Fig. 4) and a reservoir deviation from the global mean reservoir age of  $441 \pm 35$  years. This was estimated subtracting the  $^{14}C$  age value corresponding to the historical dates 1828 and 1908 CE ( $499 \pm 24$  and  $448 \pm 23$   $^{14}C$  years, respectively; Reimer et al., 2013) from the apparent  $^{14}C$  age of the foraminifers measured at depths of 5 and 10 cm for cores BTGC8 and BGGC5, respectively (Sabatier et al., 2010; Table 2).

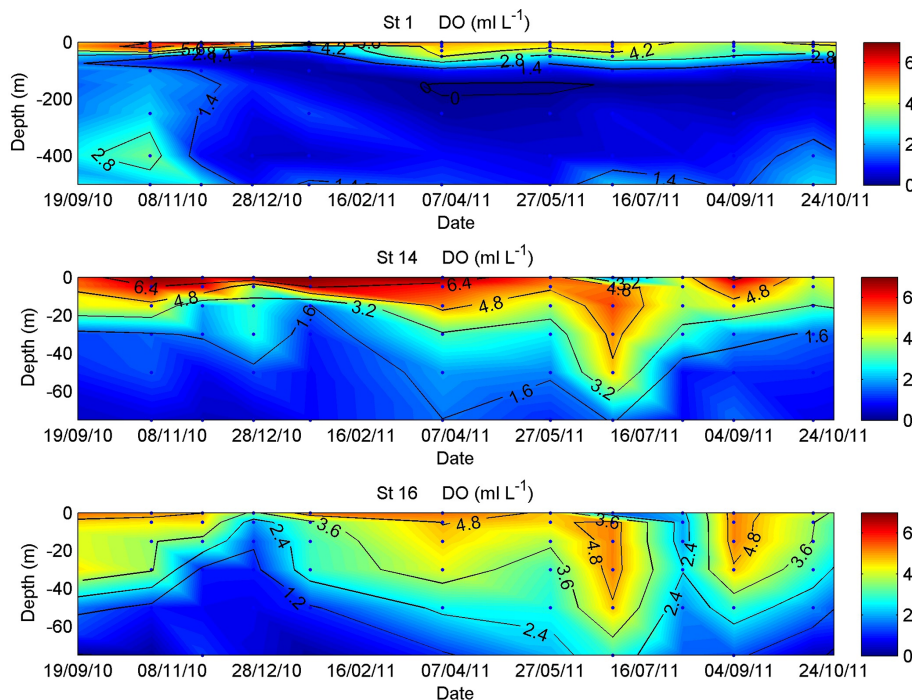


**Figure 3.** Dissolved-oxygen time series in the water column measured between October 2010 and January 2011 at stations St1, St14 and St16 off Tongoy Bay, Coquimbo (30° S).

**Table 1.** Radiocarbon dates for BGGC5 and BTGC8 sediment cores collected from mixed planktonic foraminifera and monospecific benthic foraminifera (*Bolivina plicata*), respectively. The <sup>14</sup>C-AMS was performed at NOSAMS-WHOI. The lab code and conventional ages collected from each core section are indicated. For error calculations see <http://www.whoi.edu/nosams/radiocarbon-data-calculations> (last access: 5 November 2020).

Core identification	Material	Mass (mg)	Lab code NOSAMS	Modern fraction pMC	1σ error	Conventional age (BP)	1σ error
BGGC5		Planktonic foraminifera					
10–11	Mix	1.8	OS-122160	0.8895	0.0027	940	25
18–19	Mix	1.1	OS-122141	0.7217	0.0024	2620	25
31–32	Mix	2.7	OS-122161	0.6590	0.0021	3350	25
45–46	Mix	2.0	OS-122162	0.6102	0.0017	3970	25
55–56	Mix	1.6	OS-122138	0.5864	0.0025	4290	35
66–67	Mix	2.8	OS-122304	0.5597	0.0018	4660	25
76–77	Mix	2.6	OS-122163	0.4520	0.0016	6380	30
96–97	Mix	1.1	OS-122139	0.4333	0.0033	6720	60
115–116	Mix	4.7	OS-122164	0.3843	0.0016	7680	35
BTGC8		Benthic foraminifera					
5–6	<i>Bolivina plicata</i>	4.2	OS-130657	0.8953	0.0017	890	15
20–21	<i>Bolivina plicata</i>	7.7	OS-123670	0.7337	0.0021	2490	25
30–31	<i>Bolivina plicata</i>	13.0	OS-123671	0.6771	0.0016	3130	20
40–41	<i>Bolivina plicata</i>	11.0	OS-123672	0.6507	0.0019	3450	25
50–51	<i>Bolivina plicata</i>	8.7	OS-123673	0.5877	0.0014	4270	20
60–61	<i>Bolivina plicata</i>	13.0	OS-123674	0.5560	0.0018	4720	25
71–72	<i>Bolivina plicata</i>	10.0	OS-123675	0.4930	0.0013	5680	20
80–81	<i>Bolivina plicata</i>	7.3	OS-123676	0.4542	0.0012	6340	20
90–91	<i>Bolivina plicata</i>	6.8	OS-123677	0.4259	0.0015	6860	30
96–97	<i>Bolivina plicata</i>	6.8	OS-123678	0.3903	0.0013	7560	25

**Table 2.** Reservoir age estimation considering the  $^{210}\text{Pb}$  age determined with the CRS model (McCaffrey and Thomson, 1980) at selected depth sections of the core as compared with  $^{14}\text{C}$  ages (years BP) from the Marine13.14 curve (Reimer et al., 2013) according to Sabatier et al. (2010).

Core	Depth (cm)	Age from CRS model (CE) <sup>a</sup>	Age (years BP) <sup>b</sup>	$^{14}\text{C}$ age Marine13.14	$^{14}\text{C}$ age BP from foram.	DR
BGGC5	10.5	1828	122	$499 \pm 24$	$940 \pm 25$	$441 \pm 35$
BTGC8	5.5	1908	42	$448 \pm 23$	$890 \pm 15$	$442 \pm 27$

<sup>a</sup> Common era. <sup>b</sup> Before present = 1950.

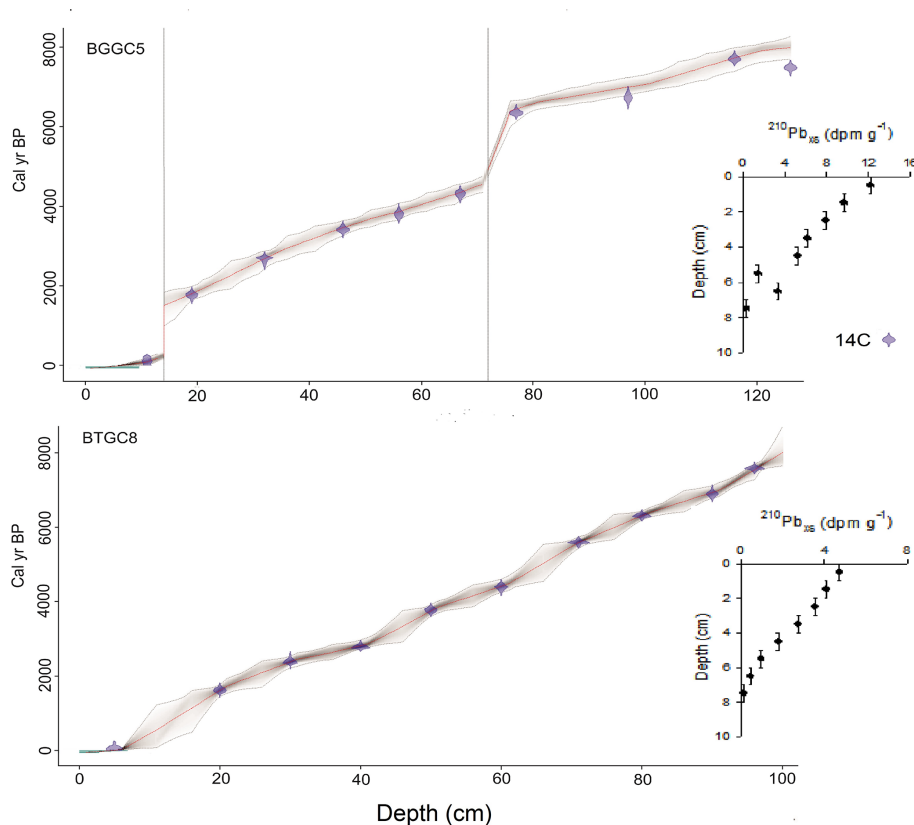


**Figure 4.** Age model based on  $^{14}\text{C}$ -AMS and  $^{210}\text{Pb}$  measurements. The timescale was obtained according to the Bacon age–depth–modeling open-source software (Blaauw and Christen, 2011) considering the Marine curve  $^{13}\text{C}$  (Reimer et al., 2013).

### 3.3 Geophysical characterization

The magnetic susceptibility ( $\text{SI} \times 10^{-8}$ ) was measured with a Bartington MS2E susceptibility meter with a surface-scanning sensor at the Sedimentology Laboratory at Centro Eula, Universidad de Concepción. Mean values from three measurements were calculated for each sample.

The grain size was determined using a Mastersizer 2000 laser particle analyzer (Hydro 2000-G, Malvern) in the Sedimentology Laboratory at Universidad de Chile. Skewness, sorting and kurtosis were evaluated using the GRADISTAT statistical software (Blott and Pye, 2001), which includes all particle size spectra.

### 3.4 Chemical analysis

Trace element analyses were performed via inductively coupled plasma mass spectrometry (ICP-MS) using an Agilent 7700x at Université de Montpellier (Observatoire des Sciences de l'Univers, OSU; L'Observatoire de recherche méditerranéen de l'environnement, OREME/Analyse des Eléments en Trace dans l'Environnement & ISotopes, AETE regional facilities). The analysis considered reference materials (UBN, BEN and MAG1) that had an accuracy higher than  $\pm 5\%$ ; the analytical precisions were between 1% and 3%. Internal standardizations with In and Bi were used to deconvolve the mass-dependent sensitivity variations in both

**Table 3.** Concentration of elements in the Pachingo wetland sediments, considered as lithogenic background for the study area. The values correspond to mean concentrations in the surface sediments (0–3 cm).

Element	Metal/Al $\times 10^3$	SD
Ca	686.5	139.3
Fe	591.3	84.5
P	8.6	0.7
Sr	5.7	0.6
Ba	5.6	0.1
Cu	0.258	0.019
Ni	0.174	0.005
U	0.020	0.003
Mo	0.020	0.003
Cd	0.0021	0.0003
Re	0.00004	0.00001

matrix and instrumental origin occurring during the course of an analytical session. The analytical precisions attained were between 1 % and 3 %.

The element concentrations were normalized using Al due to its conservative behavior that allows the assessment of the relative enrichment and depletion of elements and the evaluation of the crustal contribution for each element (Calvert and Pedersen, 2007). The authigenic enrichment factor (EF) was estimated as  $EF = (Me/Al)_{\text{sample}} / (Me/Al)_{\text{detrital}}$ , where  $(Me/Al)_{\text{sample}}$  is the bulk sample metal (Me) concentration normalized to the Al content, and the denomination “detrital” indicates a lithogenic background (Böning et al., 2009). Detrital  $([Me]_{\text{detrital}}$  and  $[Al]_{\text{detrital}})$  concentrations were established considering the local metal abundance, which is more accurate than using mean Earth crust values (Van der Weijden, 2002). We used average element concentrations on surface sediments (0–3 cm) of the Pachingo wetland (Table 3).

TOC and stable-isotope ( $\delta^{15}\text{N}$  and  $\delta^{13}\text{C}$ ) analyses were performed at the Institut für Geographie, Friedrich-Alexander-Universität (FAU) Erlangen-Nürnberg, Germany, using a Carlo Erba elemental analyzer NC2500 and an isotope ratio mass spectrometer (Delta Plus, Thermo-Finnigan) for isotopic analysis. Stable-isotope ratios were reported in the  $\delta$  notation as the deviation relative to international standards (Vienna Pee Dee Belemnite for  $\delta^{13}\text{C}$  and atmospheric  $\text{N}_2$  for  $\delta^{15}\text{N}$ ); thus,  $\delta^{13}\text{C}$  or  $\delta^{15}\text{N}$  equals  $((R_{\text{sample}}/R_{\text{standard}}) - 1) \times 10^3$ , where R is  $^{13}\text{C}/^{12}\text{C}$  or  $^{15}\text{N}/^{14}\text{N}$ , respectively. The typical precision of the analyses was  $\pm 0.1\text{‰}$  for  $\delta^{15}\text{N}$  and  $\delta^{13}\text{C}$ .

Biogenic opal was estimated following the procedure described by Mortlock and Froelich (1989). The analysis was performed by molybdate-blue spectrophotometry (Hansen and Koroleff, 1999), conducted at the laboratories of Marine Organic Geochemistry and Paleoceanography, University of Concepción, Chile. Values for biogenic opal were expressed by multiplying the Si (%) by 2.4 (Mortlock and Froelich,

1989). The analytical precision was  $\pm 0.5\%$ . Accumulation rates were determined based on the sediment mass accumulation rates and amount of opal for each core section in percent.

### 3.5 Microfossil analyses

Qualitative abundances of siliceous microfossils were determined for every 1 cm following the Ocean Drilling Program (ODP) protocol described by Mazzullo and Graham (1988). This information was used to select sections every 4, 8 and 12 cm for BGGC5 and every 6 cm for BTGC8 to determine quantitative abundances of microfossils (diatoms, silicoflagellates, sponge spicules, chrysophytes and phytoliths). Roughly 0.5 g of freeze-dried sediment was treated according to Schrader and Gersonde (1978) for siliceous microfossils. They were identified and counted under an Olympus CX31 microscope with phase contrast, in which one-fifth of the slides were counted at 400X for siliceous microfossils, and one transect at 1000X was counted for *Chaetoceros* resting spores (*Ch. RSs*). Two slides per sample were counted, with an estimated counting error of 15 %. Total diatom abundances are given in valves per gram of dry sediments.

Pollen analysis was conducted following the standard pollen extraction methodology (Faegri and Iversen, 1989). The identification was conducted under a stereomicroscope, with the assistance of the Heusser (1973) pollen catalog. A total of 100–250 terrestrial pollen grains were counted in each sample. The pollen percentage for each taxon was calculated from the total sum of terrestrial pollen (excluding aquatic taxa and fern spores). Pollen percentage diagrams and zonation were generated using the Tilia software (Grimm, 1987).

We further summarize pollen-based precipitation trends by calculating a pollen moisture index (PMI), which is defined as the normalized ratio between Euphorbiaceae (wet coastal scrubland) and Chenopodiaceae (arid scrubland). Thus, a positive (negative) value for this index point corresponds to relatively wetter (drier) conditions.

## 4 Results

### 4.1 Geochronology

The activity of  $^{210}\text{Pb}_{\text{xs}}$  (unsupported) was obtained from the surface to a depth of 8 cm in the two cores, with an age of  $\sim 1860$  CE at 8 cm in both (Table S1). Greater surface activities were obtained for core BGGC5 ( $13.48 \pm 0.41$  dpm  $\text{g}^{-1}$ ) than core BTGC8 ( $5.80 \pm 0.19$  dpm  $\text{g}^{-1}$ ), showing an exponential decay with depth (Fig. 4). A recent sedimentation rate of  $0.11 \pm 0.01$  cm  $\text{yr}^{-1}$  was estimated.

The age–depth model provided a maximum age of 7990 cal BP for core BGGC5 and 8012 cal BP for core BTGC8 (Fig. 4). A mean sedimentation rate of  $0.026 \pm 0.012$  cm  $\text{yr}^{-1}$  was estimated for core BGGC5, with a period

of relatively low values ( $<0.01 \text{ cm yr}^{-1}$ ) between 240 and 1500 cal BP and between  $\sim 5000$  and 6400 cal BP. This variation in the accumulation rates occurred over a few centimeters (5 and 7 cm, respectively); thus, this rapid decrease was considered as a hiatus in the age–depth modeling. The model assumes that the accumulation rates right before and after the hiatus are not autocorrelated, obtaining variable sedimentation rates which are more accurate to the sedimentation process. We could not resolve the length and time of hiatuses; we assumed an elapsed time of 1400 years based on the difference between the radiocarbon ages before and after the hiatus and a mid-depth corresponding to those gaps. Although we did not have stratigraphic evidence of these discontinuities in the sediment core, we believe that the assumptions considered allowed the development of reasonable age–depth models. Nevertheless, the interpretations of the proxy records were taken with caution in these age ranges. For BTGC8, mean sedimentation rates were less variable in the entire core at  $0.013 \pm 0.006 \text{ cm yr}^{-1}$ . The local reservoir deviation values were close to the global marine reservoir (Table 2) and higher than other estimations along the Chilean margin at shallower depths ( $146 \pm 25$  years at  $<30$  m water depth; Carré et al., 2016; Merino-Campos et al., 2018). Our coring sites are deeper ( $\sim 90$  m water depth) and influenced by upwelling water from Lengua de Vaca Point, which could explain such differences. However, moderate differences were observed between the models using both reservoir values. Thus, our estimations were based on two prebomb values established with  $^{210}\text{Pb}$  measured in sediments and  $^{14}\text{C}$  in foraminifers, used for the age modeling.

## 4.2 Geophysical characterization

Sediments retrieved from the bays showed fine grains within the range of very fine sand to silt in the southern areas. There, grain size distribution was mainly unimodal, very leptokurtic, more sorted and skewed to fine grain when compared with sediments from the northern areas. Sediment cores obtained from the northern areas were sandy (coarse sand and gravel), with abundant calcareous debris. Longer cores of soft sediment were retrieved at the southernmost areas (BGGC5 and BTGC8; Fig. 1), where the silty component varied between 40 % and 60 % (Fig. 5a, b). The clay component was very low for both cores ( $<2$  %). The sediment's color ranged from very dark grayish-brown to dark olive-brown (2.5Y 3/3–3/2) in Guanaqueros Bay (BGGC5) and from dark olive-gray to olive-gray (5Y 3/2–4/2) in Tongoy Bay (BTGC8). Visible macroremains (snails and fish vertebrae) were found as well as weak laminations at both cores. The magnetic susceptibility showed higher values close to the surface, up to  $127 \times 10^{-8}$  SI for BGGC5, and lower values ( $85 \times 10^{-8}$  SI) for BTGC8. At greater depths, however, the values were very constant, at  $5\text{--}8 \times 10^{-8}$  SI for core BGGC5 and  $12\text{--}20 \times 10^{-8}$  SI for core BTGC8. In both cores, susceptibility rose substantially in the last cen-

tury (Fig. 5a, b). Lower bulk densities were estimated for core BGGC5 ( $0.7\text{--}0.9 \text{ g cm}^{-3}$ ) compared with core BTGC8 ( $>1 \text{ g cm}^{-3}$ ; Fig. 5a, b). Consistent with this, the mean grain size amounted to  $60\text{--}80 \mu\text{m}$  in Guanaqueros Bay (BTGC8) compared with  $50\text{--}60 \mu\text{m}$  in Tongoy Bay (BGGC5). Both cores were negatively skewed, with values of  $-1$  to  $-1.2$  for BGGC5 and  $-1$  to  $-2.5$  for BTGC8. Minor increases toward coarser grain size were observed over the past  $\sim 1000$  years, especially in Tongoy Bay (BTGC8). In both cases, grain size distributions were strongly leptokurtic. The Ca/Fe ratio also reduced with time, except for core BTGC8, where it was only observed during the last  $\sim 2000$  years.

## 4.3 Biogenic components

### 4.3.1 Siliceous microfossils and biogenic opal

The total diatom abundance fluctuated between  $5.52 \times 10^5$  and  $4.48 \times 10^7$  valves  $\text{g}^{-1}$  for core BGGC5. This abundance showed good correlation with biogenic opal content for BGGC5 ( $R^2 = 0.52$ ,  $P < 0.5$ ), with values increasing from 72 cm to the bottom of the core, corresponding to 4900 cal BP, and reaching their highest values before 6600 cal BP. The opal percentage exhibited a maximum before 4900 cal BP (mode = 15.8 %). In contrast, the diatom abundance and biogenic opal were much lower for core BTGC8 ( $<2 \times 10^5$  valves  $\text{g}^{-1}$  and  $<3$  %, respectively). Here, the siliceous assemblage was almost completely formed by *Ch. RSs* (Fig. 6).

A total of 135 and 8 diatom taxa were identified in cores BGGC5 and BTGC8, respectively, whereby core BTGC8 registered very low diatom abundances. In general, diatoms were the most important assemblage of siliceous microfossils (96 %), followed by sponge spicules (3 %). The contributions of phytoliths and chrysophyte cysts were less than 2 % for core BGGC5. *Ch. RSs* were dominant in the diatom assemblage ( $\sim 90$  %; Fig. 6) and included the species *C. radicans*, *C. cinctus*, *C. constrictus*, *C. vanheurckii*, *C. coronatus*, *C. diadema* and *C. debilis*. Other recorded upwelling group species (mainly for core BGGC5) were *Skeletonema japonicum* and *Thalassionema nitzschioides* var. *nitzschioides* (Table S2). Other species range from 0.3 % to 6 % of the total assemblage.

### 4.3.2 TOC and stable-isotope distribution

Consistent with opal and diatoms, core BGGC5 showed higher values of TOC (between 2 % and 5 %) compared with less than  $\sim 1.5$  % for core BTGC8 (Fig. 5a, b). Furthermore,  $\delta^{13}\text{C}$  was slightly higher for core BTGC8 ( $-20$  ‰ to  $-21$  ‰) compared with core BGGC5 ( $-21$  ‰ to  $-22$  ‰). The former also shows slightly higher values of  $\delta^{15}\text{N}$  from the deeper sections to the surface of the core ( $<7$  ‰ to  $>10$  ‰). This increase was less evident for core BGGC5, with values of  $\sim 9$  ‰ at depth to  $>10$  ‰ at the surface (Fig. 5a, b). The re-



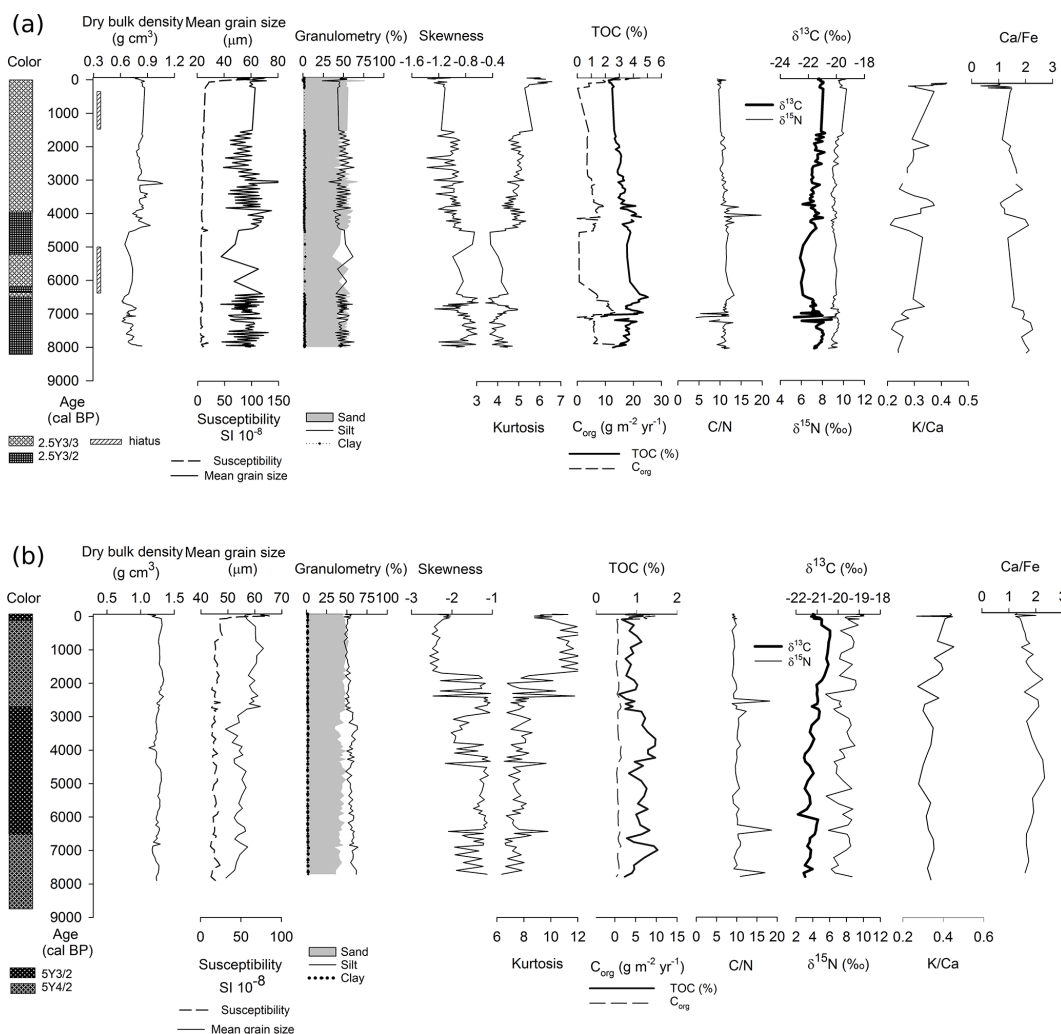


**Figure 5.** Characterization of sediment cores retrieved from (a) Guanaqueros Bay (BGGC5) and (b) Tongoy Bay (BTGC8), where the color (Munsell chart scale) represents the depth, dry bulk density, mean grain size, granulometry (percentage of sand, silt and clay), statistical parameters (skewness, kurtosis), organic components (TOC, C/N ratio, stable isotopes  $\delta^{15}\text{N}$  and  $\delta^{13}\text{C}$ ) and chemical composition (K/Ca, Ca/Fe).

duced TOC content was related to the slightly higher  $\delta^{13}\text{C}$  values (approximately  $-20\text{‰}$ ) in both cores.

### 4.3.3 Pollen record

Initial surveys of core BTGC8 (Tongoy Bay) revealed extremely low pollen abundances, which hampered further palynology work. A comprehensive pollen analysis was conducted only for core BGGC5 (Guanaqueros Bay). The pollen record of core BGGC5 consisted of 29 samples, shown in Fig. 7. The record was divided into five general zones following visual observations of changes in the main pollen types and was also assisted by CONISS cluster analysis.

Zone BG-1 (7990–7600 cal BP) is dominated by the herbaceous taxa Chenopodiaceae, *Leucheria*-type, Asteraceae

subfamily (subf.) Asteroideae and Apiaceae, with overall high values for the wetland genus *Typha* spp.

Zone BG-2 (7600–6700 cal BP) is also dominated by Chenopodiaceae, *Leucheria*-type and Asteraceae subf. Asteroideae. In addition, other nonarboreal elements, such as *Ambrosia*-type, Poaceae, Brassicaceae and *Chorizanthe* spp., increase considerably. Zone BG-3 (6700–3500 cal BP) is marked by a steady decline in Chenopodiaceae and *Leucheria*-type and by the increase in several other herbaceous elements, such as Euphorbiaceae, *Baccharis*-type and Brassicaceae.

Zone BG-4 (3500–50 cal BP) is mostly dominated by Ast. subf. Asteroideae and is marked by a decline in Chenopodiaceae and *Leucheria*-type. Other coastal taxa, such as Euphorbiaceae, *Baccharis*-type, Asteraceae subf. Cichori-

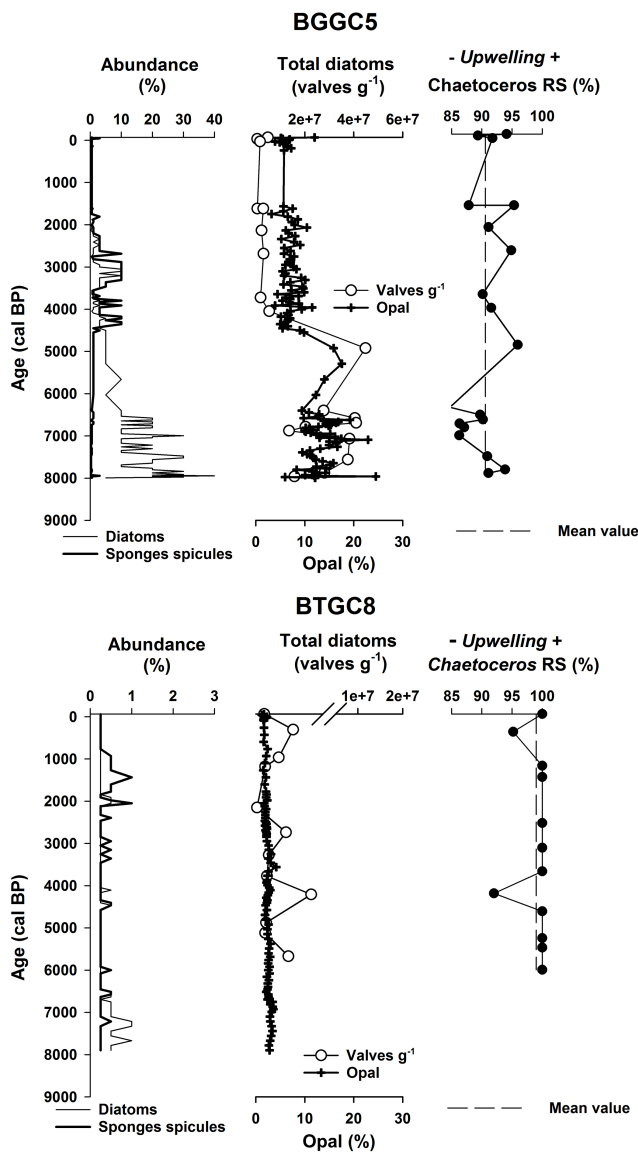


**Figure 6.** Diatom and sponge spicule relative abundances, total diatom counts (valves  $g^{-1}$ ) and opal (%), and downcore variations in *Ch. RS* percentages as proxies of upwelling intensity in cores BGGC5 and BTGC8 (Guañaqueros and Tongoy Bay, respectively). The dashed line represents the average of *Ch. resting* spores for the respective core.

oideae, *Quillaja saponaria*, Brassicaceae and *Salix* spp., also increase in this zone.

In Zone BG-5 (50 cal BP–present), the upper portion of the record is dominated by Asteraceae subf. Asteroideae and Poaceae and is marked by higher numbers of Geraniaceae specimens, Asteraceae subf. Mutisieae, Myrtaceae and *Q. saponaria*. Additionally, this zone includes introduced pollen types such as *Rumex* spp. and *Pinus* spp. The latter is not shown in Fig. 7 because its abundance was minimal.

Overall, the most distinctive trend revealed by core BGGC-5 is a long-term decline in Chenopodiaceae and higher amounts of Euphorbiaceae and Asteraceae subf. Asteroideae. Along with these changes, a further increase in several other types of pollen, representative of the coastal shrubland vegetation, began at approximately 6700 cal BP.

#### 4.4 Trace element distributions

Trace elements are presented as metal/Al ratios in Fig. 8a and b for Guañaqueros (BGGC5) and Tongoy bays (BTGC8), respectively. The metals that are sensitive to changes in the oxygen concentration (U, Re, Mo) showed an increasing metal/Al ratio from the base of core BGGC5 (~7990 cal BP) up to 6600 cal BP. After this peak, these ratios increased slightly toward 1800 cal BP, close to the beginning of the recent era, followed by a sharp reduction until present. The exception to this trend was Mo, which reached a maximum value up to 6600 cal BP and then reduced steadily to the present. Similarly, metal ratios for core BTGC8 increase over time; however, the peak was observed at ~1000 cal BP for U and Re and at 6000 cal BP for Mo, with a second minor peak at 3400 cal BP. Iron revealed a clear upward trend at 3500–3800 cal BP for core BGGC5 and a second peak between 4500 and 6500 cal BP, which was not clearly observed for the Tongoy core (BTGC8). Instead, core BTGC8 showed higher values before 6400 cal BP. In both cores, Fe increased over the past ~80 years, whereas no clear trend could be established for Mn. In general, metal/Al values were higher for core BGGC5.

A second group of elements (metal/Al ratio), including Ca, Ni, Cd and P (related to primary productivity and organic fluxes), showed a pattern similar to that of Mo/Al of core BGGC5, i.e., increasing values from ~7990 cal BP, reaching the highest values near 6600–7000 cal BP; afterwards, the values followed a constant reducing trend toward the present. Otherwise, Cu/Al (a nutrient-type element) showed a different pattern, similar to the Fe/Al distribution, with a maximum value at 3500–3800 cal BP and a conspicuous upward trend over the past ~80 years. A third group, consisting of Ba and Sr, exhibited a similar pattern but smoother, showing the maximum values before 6600 cal BP. For core BTGC8, a less clear pattern was demonstrated. Ca, Ni, Cd and P ratios for core BTGC8 showed only slightly decreasing values and very low peak values compared with core BGGC5; however, Ni/Al showed increasing concentrations over the past 80 years, which was not observed for core BGGC5. Metal/Al ratios of Ba and Sr showed no substantial variation in time. In general, all the elemental concentrations were lower in core BTGC8 than in core BGGC5 and presented similar long-term reduction patterns toward the present, except for Cu, Ni and Fe.

The authigenic enrichment, expressed as EF values, suggests a large enrichment of nutrient-type elements in a period prior to 6600 cal BP following the trend of the Me/Al ratios,

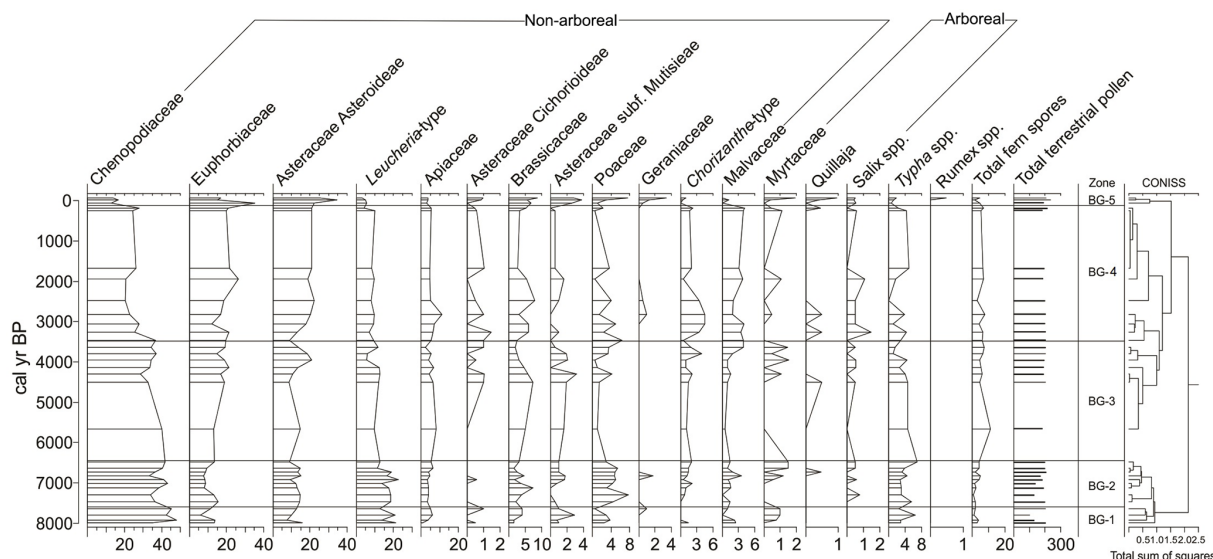


Figure 7. Pollen record in core BGGC5.

except for Ba and Fe, which did not show authigenic enrichment. The EFs exhibited a sharp decrease in enrichment in recent times after 90 cal BP (Fig. 9).

## 5 Discussion

### 5.1 Sedimentary composition of the cores: terrestrial versus biogenic inputs

The sediments in the southern zones of the bays are a sink of fine particles transported from the north and the shelf (Fig. 5a, b) and respond to water circulation in the Guanaqueros and Coquimbo bays (Fig. 1) with two counter-rotating gyres moving counterclockwise to the north and clockwise to the south (Valle-Levinson and Moraga, 2006; Fig. 1). The differences established by the sediment composition of the bays show that the sediments of Guanaqueros Bay better represent the organic-carbon flux to the bottom, with higher accumulation rates (mean value:  $16 \text{ g m}^{-2} \text{ yr}^{-1}$ ) and higher numbers of siliceous microfossils. Furthermore, it is a better zone than Tongoy for pollen identification (Figs. 5a, 6 and 7). Both areas have sediments composed of winnowed particles and relatively refractory material (C/N: 9–11), which has a slightly lower isotopic composition than the TOC composition in the water column ( $-18\text{‰}$ ; Fig. 2) and is transported by water circulating over the shelf.

The isotopic variations in  $\delta^{13}\text{C}$  and  $\delta^{15}\text{N}$  did not clearly establish differences between the sediments of the two bays; however, minor differences in  $\delta^{15}\text{N}$  would indicate a greater influence of the upwelling nutrient supply and OMZ on the shelf, resulting in a  $\delta^{15}\text{N}$  of  $9\text{‰}$ – $10\text{‰}$  in Guanaqueros Bay, values which are slightly higher than those in the Tongoy Bay sediments (Fig. 5a, b). This isotopic composition corre-

sponds to that of  $\text{NO}_3^-$  in the upwelling waters (De Pol-Holz et al., 2007) in the range of that measured in north-central Chile ( $\sim 11\text{‰}$ ; Hebbeln et al., 2000; De Pol-Holz et al., 2007, 2009). This is due to the isotopic fractionation of  $\text{NO}_3^-$  during nitrate reduction within the OMZ, which leaves remnant  $\text{NO}_3^-$  enriched in  $^{15}\text{N}$  (Sigman et al., 2009; Ganeshram et al., 2000, and references therein). This is particularly relevant because it demonstrates the relevance of the OMZ over the shelf sediments off Coquimbo at shallow depths and the influence of the poleward undercurrent from the Peru OMZ (Mollier-Vogel et al., 2019).

For sediment core BTGC8, lower values ( $<8\text{‰}$ ) measured at greater depths within the core should account for a mix with isotopically lighter terrestrial organic matter (Sweeney and Kaplan, 1980), owing to its proximity to a small permanent wetland on the southern side of Tongoy Bay (Pachingo), the sediments of which have  $\delta^{15}\text{N}$  of  $2\text{‰}$ – $6\text{‰}$  (Muñoz et al., unpublished data). This suggests that the Tongoy sediments contain a greater proportion of continental material compared to Guanaqueros Bay (Fig. 5b).

Thus, cores BGGC5 and BTGC8 in the Guanaqueros and Tongoy bays record the variability in oceanographic conditions; however, in the Tongoy core, the concentration of oceanographic proxies is diluted owing to the input of terrigenous material. This helps to decipher the climatic variability, considering that the main input of clastic material to the area takes place during major flooding events. Additionally, the main circulation of the bay system leads to favorable conditions for the sedimentation and preservation of organic marine proxies in Guanaqueros Bay, making the sedimentary records of these sites complementary.

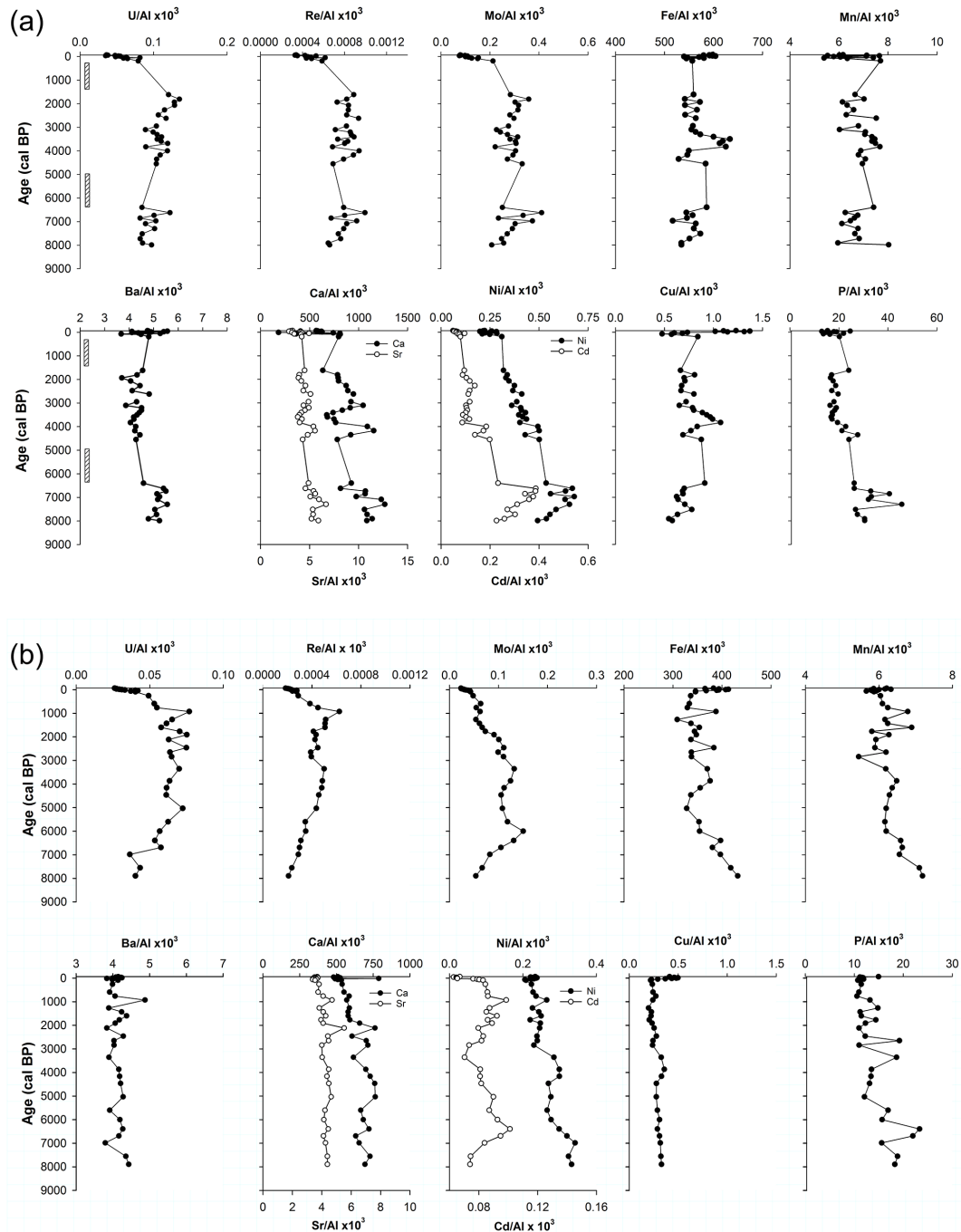


**Figure 8.** Downcore trace element variations in (a) Guanaqueros Bay (BGGS5) and (b) Tongoy Bay (BTGC8), off Coquimbo (30° S).

## 5.2 Temporal variability of primary productivity and the oxygenation of bottoms

Ca, Sr, Cd and Ni profiles suggest a lower share of organic deposition over time (Fig. 8a, b), consistent with the slight reduction in TOC content observed in the sediments (Fig. 5a, b) and concomitant with the other elements related to organic fluxes to the bottom and primary productivity. Similarly, the

maximum Ba concentrations indicate higher productivity before 6600 cal BP. The same is true for Ca, Cd and Ni, suggesting that the maximum productivity and organic fluxes to the bottom occurred during this period. After this age, the reduction in TOC and other nutrient-type elements (Ni, Sr, Ca, Cd) to the present is consistent with the increase in oxygen at the bay bottom.

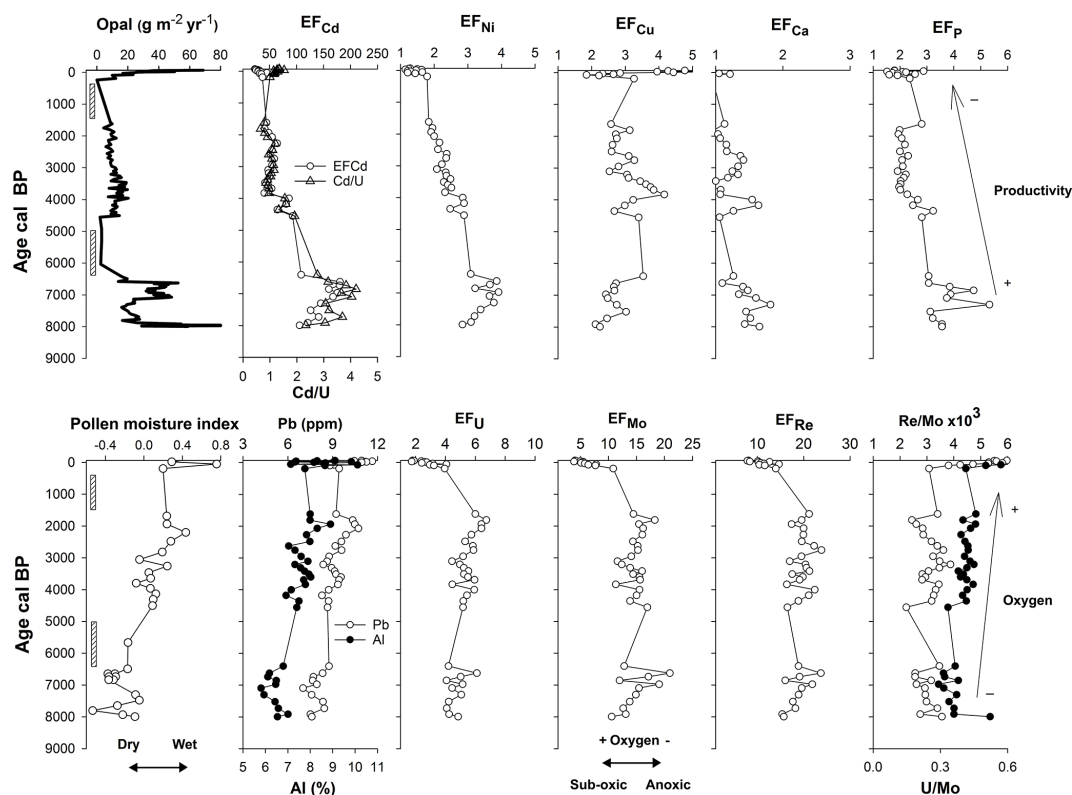


**Figure 9.** Opal accumulation and authigenic enrichment factor (EF) of trace elements calculated for Guanaqueros Bay (core BGGC5). Lithogenic background was estimated from the surface sediments of Pachingo wetland cores (see text). Pollen moisture index defined as the normalized ratio between Euphorbiaceae (wet coastal shrubland) and Chenopodiaceae (arid scrubland). Positive (negative) values for this index indicate the relative expansion (reduction) of coastal vegetation under wetter (drier) conditions. Pb and Al distribution for core BGGC5, representative of terrigenous input to the bay.

The slight rise in Ba in the last  $\sim 115$  years (Fig. 8a) is a response to a less anoxic environment, owing to better preservation within the sediments in less anoxic environments with moderate productivity (Torres et al., 1996; Dymond et al., 1992), as is the case with our study site (gross primary productivity =  $0.35$  to  $2.9$  g C m<sup>-1</sup> d<sup>-1</sup>; Daneri et al., 2000). This leads to a negative correlation with TOC ( $-0.59$ ; Table 4), owing to the remobilization of Ba under anoxic conditions before 6600 cal BP. Meanwhile, the P distribution showed a trend similar to that of TOC and the other elements related to the organic fluxes to the bottom (Ni, Cd), although with a lower correlation ( $\sim 0.6$ ). This is consistent with the distributions observed for U, Re and Mo for core BGGC5, which indicate that anoxic or suboxic conditions were developed from 7990 to 1800 cal BP but were stronger before 6600 cal BP (Fig. 8a, b). After this period and to the present, a remarkable reduction in their concentration suggests a more oxygenated bottom environment, concurrent with lower organic fluxes to the sediments. The Re profile shows the influence of suboxic waters not necessarily associated with higher organic-matter fluxes to the bottom. Since this element is not scavenged by organic particles, its variability is directly re-

lated to oxygen changes (Calvert and Pedersen, 2007, and references therein).

Otherwise, the accumulation of P depends on the deposition rate of organic P (dead plankton, bones and fish scales) on the bottom and is actively remineralized during aerobic or anaerobic bacterial activity. P and TOC showed a declining trend toward the present, suggesting a reduction in flux of organic matter over time, which was also observed for Ni and Cd distributions. Alternatively, the reducing fluxes of organic matter could be explained by the higher remineralization of organic material settled at the bottom due to higher oxygen availability, as shown by U, Mo and Re distributions (Fig. 8a, b). However, the lower  $\delta^{15}\text{N}$ , depending on the denitrification process, is similar to that at deeper environments in the zone (De Pol-Holz et al., 2009), suggesting that the influence of the reductive environment of the OMZ over the shelf and changes in U, Mo and Re records could depend mainly on the OMZ variability. Thus, the influence of the primary productivity on oxygen consumption at the bottom over time would be secondary in this system, which is considered to be moderated in productivity compared with upwelling centers in northern and southern Chile.

**Table 4.** Spearman rank order correlations for geochemical data. Significant values >0.8 are indicated in bold.

BGGC5																
	Al	P	K	Ca	Mn	Fe	Ni	Cu	Mo	Cd	Re	Sr	U	Ba	Opal	TOC
Al	1.00	-0.62	0.49	-0.48	0.64	0.60	-0.75	0.56	-0.10	-0.73	-0.08	-0.33	0.08	0.49	-0.52	-0.44
P		1.00	-0.31	0.37	-0.45	-0.56	0.56	-0.57	0.01	0.61	-0.11	0.39	-0.12	-0.20	0.49	0.24
K			1.00	-0.24	<b>0.90</b>	<b>0.83</b>	-0.29	0.47	0.28	-0.42	0.33	-0.12	0.50	0.26	-0.25	-0.19
Ca				1.00	-0.47	-0.50	0.44	-0.64	0.23	0.59	0.39	<b>0.92</b>	0.30	-0.60	0.18	0.32
Mn					1.00	<b>0.94</b>	-0.51	0.68	-0.01	-0.68	0.07	-0.32	0.24	0.43	-0.39	-0.31
Fe						1.00	-0.49	<b>0.81</b>	0.03	-0.70	0.11	-0.40	0.23	0.36	-0.37	-0.21
Ni							1.00	-0.51	0.49	<b>0.91</b>	0.35	0.25	0.26	-0.70	0.72	0.64
Cu								1.00	-0.12	-0.71	-0.06	-0.61	0.00	0.31	-0.39	-0.07
Mo									1.00	0.50	<b>0.88</b>	0.10	<b>0.91</b>	-0.48	0.33	0.36
Cd										1.00	0.36	0.42	0.27	-0.67	0.70	0.54
Re											1.00	0.27	<b>0.92</b>	-0.50	0.16	0.38
Sr												1.00	0.24	-0.36	0.05	0.17
U													1.00	-0.39	0.10	0.29
Ba														1.00	-0.30	-0.59
Opal															1.00	0.35
TOC																1.00

BTGC8																
	Al	P	K	Ca	Mn	Fe	Ni	Cu	Mo	Cd	Re	Sr	U	Ba	Opal	TOC
Al	1.00	-0.19	-0.17	-0.37	-0.02	-0.03	-0.39	-0.04	-0.39	0.02	-0.13	-0.58	-0.19	0.07	-0.41	-0.29
P		1.00	0.23	0.00	0.43	0.28	0.58	0.23	0.37	0.13	-0.04	0.30	0.14	-0.14	0.56	0.13
K			1.00	-0.02	0.54	0.41	0.43	0.22	-0.11	0.05	-0.04	0.19	-0.28	0.28	0.26	0.20
Ca				1.00	-0.33	-0.27	0.00	-0.23	0.39	0.01	0.33	0.50	0.47	-0.34	0.20	0.34
Mn					1.00	0.21	0.64	0.01	0.05	0.33	0.15	0.32	-0.02	0.24	0.32	0.00
Fe						1.00	0.13	0.71	-0.40	-0.48	-0.67	-0.37	-0.62	0.13	0.14	0.10
Ni							1.00	0.24	0.56	0.20	0.25	0.64	0.19	-0.16	<b>0.80</b>	0.45
Cu								1.00	-0.25	-0.68	-0.56	-0.22	-0.61	-0.10	0.21	0.37
Mo									1.00	0.45	0.59	0.66	0.69	-0.41	0.58	0.30
Cd										1.00	0.56	0.39	<b>0.52</b>	0.11	0.10	-0.12
Re											1.00	0.53	<b>0.83</b>	-0.16	0.13	0.17
Sr												1.00	0.58	-0.13	0.52	0.23
U													1.00	-0.19	0.21	0.00
Ba														1.00	-0.28	-0.42
Opal															1.00	0.39
TOC																1.00

Productivity reconstructions were based on the qualitative relative abundances of diatom and sponge spicules, quantitative diatom counts (valves  $\text{g}^{-1}$ ), and biogenic opal content only in core BGGC5 since core BTGC8 registered low valve counts (<1% in relative diatom abundance). However, in both cores, diatom assemblages were represented mainly by *Ch. RSs*, which are used as upwelling indicators (Abrantes, 1988; Vargas et al., 2004). The downcore siliceous productivity based on opal distribution (Figs. 6 and 9) distinguished three main time intervals of higher productivity, which coincided with the ages highlighted by the distribution of the sedimentary proxies noted previously: (1) >6600 cal BP, (2) 4500–1800 cal BP and (3) ~140 cal BP to recent times (2015 CE). Other periods between 6600 cal BP and 4500 cal BP and between 1800 cal BP and 140 cal BP did not experience higher productivities.

In the first period (>6600 cal BP), the opal accumulation rate was remarkably high, amounting to  $\sim 35 \pm 18 \text{ g m}^{-2} \text{ yr}^{-1}$  (range: 16–119  $\text{g m}^{-2} \text{ yr}^{-1}$ ; Fig. 9) when *Chaetoceros* spores were predominant, indicating an intensification in upwelling. During this period, all metal proxies suggest that primary productivity increases before 6600 cal BP, owing to the high

concentrations and major enrichment of Ni, Ca and P that occurred in this period, concomitant with higher opal accumulation within the sediments (Figs. 6 and 9). From these elements, Ni is the best indicator of organic sinking flux related with diatom productivity in organic-rich upwelling sediments (Böning et al., 2015), which helps to sustain our statement. In addition, the authigenic enrichments of Cd were very high (>100; Fig. 9) resulting in high Cd/U ratios (>2; Fig. 9), indicative of anoxic conditions as this ratio could vary between 0.2 and 2, from suboxic to anoxic environments (Nameroff et al., 2002). The Cd accumulation in this period was higher than that reported for a highly productive zone off Concepción in periods of high organic-carbon accumulation in the sediments (~5; Muñoz et al., 2012). Additionally, the high enrichment of Mo (~20) indicates the prevalence of anoxic conditions at the bottom in this period due to the control by sulfide concentrations (Huerta-Díaz and Morse, 1992; Chaillou et al., 2002; Nameroff et al., 2002; Sundby et al., 2004; Tribouillard et al., 2004). Our low U/Mo ratio (~0.3; Fig. 9) is similar to those values reported today in shallower anoxic zones off Peru interrupted by seasonal oxygenation (McManus et al., 2006; Scholz et al., 2011, Sal-

vatteci et al., 2016; Vergara et al., 2016). This resembles our shelf, notwithstanding the prevalence of very reduced conditions within the sediments.

The enhanced reduced conditions, probably sulfidic, before 6600 cal BP favored the accumulation of Mo and Cd over that of U occurring in anoxic environments, where the chemocline is close to the water–sediment interface or above it, allowing the formation of authigenic Mo that exceeds the U uptake within the sediments (Algeo and Tribovillard, 2009, and references therein). Re is enriched in less reduced conditions than Mo, resulting in the lowest Re/Mo in this period (Fig. 9). This is congruent with the environmental conditions at the bottom in zones of high productivity and intense upwelling, where sulfidic conditions are developed owing to oxygen consumption in the shallower zones and linked to the OMZ, as in northern Chilean regions, where the main productivity is developed over the narrow shelf. Thus, the high productivity before 6600 cal BP could result from a more intense upwelling that generated permanently reduced conditions that became very anoxic at the bottom in this period. Even so, the low-oxygen conditions prevailed in the subsequent periods but were less intense than before.

After 6400 cal BP until 4500 cal BP, we obtained little information owing to a gap in the sedimentary record, which made it difficult to visualize changes in the oxygenation and productivity proxies in this interval. However, in the next period (4500–1800 cal BP), we observe that the opal accumulation was lower than in the previous recorded period,  $12 \pm 4 \text{ g m}^{-2} \text{ yr}^{-1}$  (range:  $6\text{--}20 \text{ g m}^{-2} \text{ yr}^{-1}$ , peaking at 3400–4000 cal BP; Fig. 9), which is partially consistent with nutrient-type element distributions and element enrichment (Figs. 8a and 9). Fe clearly shows higher values at approximately 3500 cal BP (Fig. 8a), which helped to boost primary productivity at this time, with a small increase in diatoms (valves  $\text{g}^{-1}$ ) and abundance (%; Fig. 6). Other elements showed less prominent accumulations (Ni, Cd, Ba, Ca and P), pointing to a lower organic-matter deposition into the sediments during this period (Fig. 8a). Thus, a decreasing trend in the primary productivity from 6600 cal BP is observed, which is also consistent with observations off south-central Chile ( $36^\circ \text{ S}$ , Concepción shelf), where lower accumulations of nutrient-type elements were also observed at 3600–4000 cal BP and 2600 cal BP than at 6200 cal BP (Muñoz et al., 2012).

The low-oxygen conditions within the sediments were maintained despite the downward trend in the primary productivity. This could be more related to the manifestation of the OMZ close to the coast than the oxygen consumption during organic-matter remineralization, favoring Mo and Re accumulation until 1700–1800 cal BP (Fig. 8a). Lower Cd/U ratios ( $\sim 1$ ; Fig. 9) were estimated, suggesting higher variations in the primary productivity but with moderate changes in the oxygen conditions at the bottom. High Re/Mo and U/Mo ratios could indicate a shift toward less reduced conditions but still anoxic since U, Re and Mo are highly en-

riched (6, 20 and 15, respectively; Fig. 9). U and Re accumulations occur in conditions that exhibit less intense reduction but are not very favorable for Mo accumulation (Morford et al., 2009). This could be caused by a lower C rain rate due to lower productivity, producing low oxygen consumption and a less sulfidic environment along the central Chilean margin ( $30\text{--}36^\circ \text{ S}$ ), which is in agreement with the lower biogenic opal flux and diatom abundance after 6600 cal BP (Figs. 6, 9).

Slight increasing values of Re/Mo ratios until  $\sim 3500$  cal BP suggest a decreasing trend in the reduced conditions, which became stronger after 1800 cal BP. This time was also highlighted in the sedimentary records off the Concepción shelf ( $36^\circ \text{ S}$ ; Muñoz et al., 2012), showing maximum enrichment of U and Cr near 1800 cal BP, both indicating less reduced conditions toward the present compared with previous periods. After this age, no comparison could be made owing to a discontinuity in the sedimentary records off Concepción. Nevertheless, the suboxic conditions have prevailed until today in central Chile, where the oxygenation seems to have been stronger off Coquimbo. It could be caused by eddies related to the instabilities of the Peru Undercurrent (Vergara et al., 2016), which seem to start operating more frequently from 1800 cal BP to the present. After this age to 140 cal BP, higher productivities were not found, and a second discontinuity (1500–240 cal BP) impeded environmental reconstructions, with the very low estimated sedimentation rate hindering the realization of sufficient time resolution for the proxies in this interval.

After  $\sim 140$  cal BP to recent times (2015 CE; third period mentioned before), the productivity increased substantially, deduced from the rise in opal accumulations toward the present (mean opal value of  $29 \pm 17 \text{ g m}^{-2} \text{ yr}^{-1}$ , range of  $10\text{--}69 \text{ g m}^{-2} \text{ yr}^{-1}$ ; Fig. 9); however, this corresponded with lower diatom abundances, which were observed from 1800 cal BP to the present (range:  $0.5\text{--}4.9 \times 10^6$  valves  $\text{g}^{-1}$ ; Fig. 6). This is likely caused by the fact that only a few sections of the core in this interval were analyzed for diatoms, leading to a low resolution for this measurement in the most recent period. Another possibility is that the opal flux was overestimated owing to the fact that the flux calculations were based on recent sedimentation rates, an estimation that tends to be higher than at longer timescales (Sadler et al., 1999). However, the slight increase in the Cd/U ratio, Ba concentrations and P enrichment could suggest an increase in the primary productivity and organic fluxes to the bottom in more recent times (Figs. 8, 9). In addition, the main trend established before and after the hiatus indicates an increase in the marine productivity, which would not be as high as in the first period (before 6600 cal BP). After 1800 cal BP, there is an evident change to a less reduced environment toward the present, suggesting a more oxygenated bottom environment concurrent with a reduction in primary productivity, except for the last 140 years, when the productivity has been more variable, with a slight increasing trend.

Contrary to other metals, there is a conspicuous upward trend for Cu/Al, Fe/Al and Mn/Al in recent times, which is consistent with the decreasing trend of EFs of Re, U and Mo (Figs. 8a, b and 9); these estimations would not be influenced by the sedimentation rates but rather the presence of oxygen. Otherwise, the highest enrichment of Cu could suggest the presence of particulate forms and oxide formation (Peacock and Sherman, 2004; Vance et al., 2008; Little et al., 2014) occurring in the presence of an oxygenated environment that results in a high metal enrichment of Cu ( $EF_{Cu} = 4.6 \pm 0.5$ ; Fig. 9); however, suboxic conditions have prevailed, indicated by the U/Mo ratios in the range of the reduced sediments, which are less than in the sediments of the Peru shelf (Scholz et al., 2011; Salvatelli et al., 2016). In addition, the Cu enrichment coincides with the growing trend of industrialization in the area, mainly mining activities, which has been the main economic source for the Coquimbo region since 1890; therefore, the exposition of mineral ores and mine residues to the environment by natural processes such as interperization and wind transportation deserves attention.

We suggest that the slightly higher productivity in the last 140 years has occurred in a more oxygenated environment, which seems contradictory. However, similar OMZ weakening has been described off central Peru from 1875 to 2004, caused by a balance between the local productivity and the subsurface ventilation of the intermediate circulation, operating at a (multi)decadal to centennial scale and hence related to the Interdecadal Pacific Oscillation (IPO) and ENSO (Cardich et al., 2019). Current studies have shown that changes in both the Peru–Chile Undercurrent (PCUC) and mesoscale eddy field contribute to the modulation of the vertical and offshore extension of the OMZ at intraseasonal and seasonal timescales off central Chile (e.g., Vergara et al., 2016; Frenger et al., 2018; Pizarro-Koch et al., 2019) and possibly at lower frequencies, modulating the influence of the OMZ over the coastal zones. In addition, ENSO has been identified as an important mechanism of the OMZ ventilation in the tropical southeastern Pacific through horizontal and vertical eddy fluxes; thus, during El Niño, the coastal trapped waves propagate poleward, and the water column becomes oxygenated and contrarily, during La Niña-like conditions, deoxygenated (Espinoza-Morriberón et al., 2019, and references therein).

Several observations made at the central Peruvian and south-central Chilean coasts (12–36° S) reveal that the present-day wet and dry variability associated with ENSO has a strong impact on the benthic communities. During El Niño, the large increase in the oxygen levels changes the biogeochemical processes at the bottom, and its effects can be observed several months after the event (Ulloa et al., 2001; Escribano et al., 2004; Gutiérrez et al., 2006, 2008; Sellanes et al., 2007). Thus, the increased frequency and intensity of El Niño in recent centuries would result in a mean effect, which is observed as a gradual change in metal enrichment

over time. This is explained by the episodic oxygenation, which changes the original extent of the accumulation of sensitive redox trace element through their remobilization to soluble forms (Morford and Emerson, 1999; Morford et al., 2009).

The strong trend towards increasingly reduced conditions in the northern margin of the SE Pacific (Peru and north of Chile) in the past decades has been explained by a greater impact of local productivity on coastal hypoxia (Cardich et al., 2019; Díaz-Ochoa et al., 2011), something that is not clearly observed in our records. Contrarily, a gradual oxygenation in the north-central Chilean margin was observed, which may rather respond to the deepening of the OMZ. The oxygenation and deoxygenation mechanism can be the result of coastal trapped waves, originating from the Equator and propagating along the coast, at different timescales and intensities. These modify the stability of the regional current system and the pycnocline and can trigger extratropical Rossby waves (Pizarro et al., 2002; Ramos et al., 2006, 2008), contributing to the oxygen variability in coastal zones with major impacts on redox-sensitive elements in the surface sediments.

### 5.3 Main climatic implications

According to paleoenvironmental records, the past climate and oceanographic variability has been interpreted mainly based on the past variability in the intensity of the SWWs and latitudinal position of the ITCZ (Veit et al., 1996; Hebbeln et al., 2002; Lamy et al., 1999; Maldonado and Villagrán, 2002). The ITCZ movements from the northernmost or southernmost latitudinal position depend on the different phases of ENSO and PDO variability (Yang and Oh, 2020) as the main regulators of the climate at the centennial and decadal scales. This has an impact on relevant oceanographic characteristics, such as sea surface temperature (SST), upwelling and, accordingly, productivity in the SE Pacific. We established marked differences in paleoproductivity proxies and paleo-oxygenation in the last ~ 8000 years (Figs. 6, 8), indicating that high marine productivity prevailed during our first period (8000–6600 cal BP) according to what was established for central Chile between 10 and 5 kyr ago owing to sustained mean La Niña-like conditions associated with the cold phase of the PDO (positive phase; De Pol-Holz et al., 2006; Kaiser et al., 2008; Lamy et al., 2010), concomitantly with reduced ENSO variability and a northward ITCZ displacement, which implies more permanent southeast trade winds and, hence, the upwelling of rich-nutrient cold waters in the eastern Pacific (Koutavas and Lynch-Stieglitz, 2004; Koutavas and Joanides, 2012).

Our high-productivity records associated with low-oxygen conditions at the bottom, both reaching a maximum level at 6600 cal BP, correspond to the most productive period and the most reductive environment at the bottoms over the past 8000 years. The continental climate during this period has



been described as being drier, with the predominance of La Niña-like conditions according to the northerly position of the ITCZ, which promote strong upwelling due to persistent southeast trades. This climatic condition has been described for the tropical Pacific and SE Pacific (Lamy et al., 2001; Carré et al., 2012; Koutavas et al., 2006; Salvatelli et al., 2019), indicating that La Niña-like conditions, developed during the mid-Holocene, resulted from an intensification of the SPSA and the Walker circulation. These environmental conditions are in agreement with the observations of our pollen records and productivity proxies (PMI; Fig. 9), establishing favorable conditions for upwelling and development of primary productivity along the southeastern Pacific margin.

For central Chile, the aridity conditions were limited until 5700 cal BP (Jenny et al., 2002; Maldonado and Villagrán, 2006) or 4200 cal BP (Maldonado and Rozas, 2008; Maldonado and Villagrán, 2002, 2006), characterized by reduced rainfall but intense coastal humidity, which have been associated with coastal fogs that frequently occur during the spring owing to a strengthening of the SPSA (Vargas et al., 2006; Garreaud et al., 2008; Ortega et al., 2012) and La Niña-like conditions, which explains the main variability of the SPSA (Ancapichún and Garcés-Vargas, 2015). Similarly, for southern Chile (41° S; Lamy et al., 2001), less humid conditions were described for a period between 7700 cal BP and 4000 cal BP, being stronger between 6000 cal BP and 5300 cal BP, by a poleward position of the southern westerlies. All of this points to drier conditions during the mid-Holocene, which was closely related to SPSA intensification and the southern position of the southern westerlies.

Consistent with this, a reduced ENSO variance during the early and mid-Holocene has been suggested (Rein et al., 2005), indicating a less frequent or less intense warm anomaly related to a central Pacific (CP)-mode ENSO, which produces a moderate El Niño events in the CP and strong La Niña off Peru (Carré et al., 2014; Mollier-Vogel et al., 2019). This was favorable for upwelling and primary productivity development along the Chilean and Peruvian margin. In addition, Braconnot et al. (2012) indicated that this lower ENSO was linked to freshwater melting that counteracted the insolation regime, pointing to a more limited cold and dry period between 6700 and 7500 years ago, which matches our records of maximum productivity (Figs. 6, 9) concomitantly with the lowest bottom oxygen conditions and indicates a greater influence of the OMZ over the shelf at the central Chilean margin.

After the maximum productivity recorded, a decreasing trend occurred under warm and humid climatic conditions, which would be because of an enhancement in regional precipitation in the northern margin of the SWWs (Jenny et al., 2003; Maldonado and Villagrán, 2006), consistent with the southern movement of the ITCZ, leading to wetter climatic conditions in the southern tropic regions (Koutavas and Lynch-Stieglitz, 2004). A gradual rise in K/Ca, Fe, Al and

Pb distributions was observed in our cores (Figs. 5, 9), usually considered to be an indicator of continental input by fluvial or aerial transport (Calvert and Pedersen, 2007; Kaiser et al., 2008; Govin et al., 2012; Ohnemus and Lam, 2015; Saito et al., 1992; Xu et al., 2015). This indicated that the precipitation has been increasing through the middle and late Holocene, except for a period of reduced (or weak) ENSO activity reported between 6000 and 4000 cal BP (Koutavas and Joanides, 2012; Carré et al., 2014). It is also consistent with the pollen records of central Chile, which suggest an arid phase from 6200 cal BP until 4200 cal BP (Maldonado and Villagrán, 2006). The lack of records between these ages in our cores (hiatus) prevented the search for evidence to account for this period; consequently, no sharply contrasting dry or humid periods were identified after 6600 cal BP. Mostly, a gradual increase in humidity and a weakening in paleoproductivity proxies after 4500 cal BP (Figs. 8, 9) were observed, which would be consistent with the beginning of higher ENSO variability for central Chile after 5700 cal BP (Jenny et al., 2002; Maldonado and Villagrán, 2002, 2006).

In general, the weakening of the SPSA results in an equatorward position of the southern westerlies, increasing the humidity conditions in central Chile (Lamy et al., 2001). The ENSO variability increased from 5700 cal BP, and stronger El Niño events would begin after 4000–4500 cal BP, concomitant with the high variability of latitudinal displacements of the ITCZ related to the seasonality of insolation described for the region during the middle and late Holocene (Haug et al., 2001; Toth et al., 2012; Carré et al., 2014). This is consistent with the occurrence of alluvial episodes in the area caused by more frequent or heavier rainfall events over time related to intensified westerlies and increased El Niño events observed from Peru to south of Chile (Lamy et al., 2001; Jenny et al., 2002, 2003; Rein et al., 2005; Sandweiss et al., 2007; Ortega et al., 2012, 2019). A consequence is greater continental input, as suggested by our sedimentary records in agreement with the pollen moisture index that indicated more humid conditions through the mid-Holocene to the present. This was concomitant with greater oxygenation at the bottom and reduced primary productivity. Nonetheless, between 4500 and 3000 cal BP, a slight increase in diatom abundance and opal concentrations was observed along with a slight accumulation in nutrient elements (Ni, Cd, Fe and Ca concentrations; Fig. 8). Small increases in the organic-carbon flux and Cd/U ratios (Figs. 5, 9) suggest that the increase in primary productivity could be boosted by continental nutrients (Dezileau et al., 2004; Kaiser et al., 2008). This period has been documented for the tropical eastern Pacific as a peak of La Niña activity (3000–4000 cal BP; Toth et al., 2012). This would also explain the increase in the productivity proxies.

Despite the dominance of warm events described from the middle to late Holocene, they were not strong enough to change the suboxic conditions at the bottom in the north-central Chilean margin, which varied little until 1800 cal BP

(Figs. 8, 9; see U, Mo and Re). Actually, the periodicity of El Niño was similar between 5000 cal BP and 3000 cal BP and lower than modern times (Sandweiss et al., 2007), supporting the observation of relatively low variability of the oxygen proxies in the sediments dependent on the OMZ influence over the shelf. This implies that the upper-limit location of the OMZ did not drastically change during most of the middle and late Holocene. Contrary to our observations, the sediments at the Peruvian shelf were less reduced in the late to mid-Holocene than at present, which was due to a deepening in the OMZ by the increased advection of waters enriched in oxygen from the Equatorial Undercurrent and the shifting of the OMZ center toward the Chilean margin, leaving lower  $\delta^{15}\text{N}$  values in sedimentary records off Peru (Mollier-Vogel et al., 2019). Therefore, the enhanced oxygenation of Peru and OMZ deepening translated into a decrease in the oxygen conditions off north-central Chile. This period is followed by an increased El Niño frequency that has been consistent with the intensification and frequency of flooding events recorded in Peru and central Chile in the last  $\sim 2000$  years (Rein et al., 2005; Sandweiss et al., 2007; Jenny et al., 2002; Toth et al., 2012), which is concomitant with the drastic oxygenation at the bottom observed in our records after 1800 cal BP. In this regard, the oxygen variation at the bottom would be related to a less intense effect of the OMZs over the shelf at the central Chilean margin during the warm El Niño-like phases, owing to a deepening of the oxycline (and vice versa during La Niña). These tend to be associated with low productivity and, in turn, a reduction in the organic fluxes and oxygen consumption during organic-matter diagenesis.

After 1800 cal BP, few records were obtained until 140 cal BP, when we observed the restoration of more reduced conditions, although lower than during previous periods. This corresponds to the time of Peruvian upwelling shift due to the northward displacement of the ITCZ to the modern position and the enhancement of the Walker circulation (Gutiérrez et al., 2009), which establishes an intensification of the upwelling in the eastern Pacific and consequently an increase in the primary productivity, producing high demand for oxygen during organic-matter remineralization, as observed today, which leads to stronger oxygen consumption in the northern part of the eastern margin. Nevertheless, the reduced conditions off Coquimbo in recent decades are not comparable to the environmental conditions of the Peruvian margin, where stronger deoxygenation has been developed at the bottom.

## 6 Conclusions

Our results suggest that the geochemistry and sedimentary properties of the coastal shelf environments in north-central Chile have changed considerably during the Holocene period, suggesting two relevant changes in the redox conditions and productivity, which point to a more reducing en-

vironment and higher productivity around 6600 cal BP. Afterwards, a less reducing environment along with decreasing trends in primary productivity and increased humid conditions occurs with time. The oxygenation of the surface limit of the OMZ has been proposed as the main mechanism that controls the reduced conditions over the shelf and slope sediments during the mid-Holocene, which mainly affected the Peruvian margin close to the OMZ edge. This led to contrasting conditions with the central Chilean margin, where more reducing conditions were observed, which were maintained with low variability until 1800 cal BP. After this age, the OMZ expression over the shelf was weak, returning to more reduced conditions in recent times (last 2 centuries), similar to the Peruvian margin but weaker in north-central Chile.

The northward shifts of the SWW belt, in addition to an increased frequency in El Niño events, have been proposed as the main drivers for climatic conditions during this period. These elements have introduced high variability in the primary productivity during this time interval. This also impacted the accumulation of organic matter due to an intensification of its remineralization, showing a decreasing trend in the buildup of nutrient-type elements and organic-carbon burial rates toward the present. Otherwise, decreasing oxygen content at the bottom is highly influenced during El Niño events, something that seems to have been operating at higher frequencies after 1800 cal BP and especially after 140 cal BP, when the most extreme events become more frequent. Thus, the El Niño phenomenon and ITCZ latitudinal displacement have greatly contributed to the climatic and oceanographic features in the eastern Pacific, linked to the positive or negative phases of the PDO, which all has a relevant effect on the OMZ position in the Chilean margin. Otherwise, oxygenation or deoxygenation changes can result from coastal trapped waves that can operate at different timescales and intensities and have a strong effect on the stability of the regional current system and the pycnocline position in the coastal zones.

Finally, these changes highlight the sensitivity of these environments to climate variability at different timescales, which is consistent with the description of past regional climatic trends. Based on the dramatic changes observed in the past centuries, future changes are expected in the context of global warming at unprecedented rates.

*Data availability.* The data set is available free of charge at the National Hydrographic and Oceanographic Data Center of Chile (CENDHOC) through the portal [http://www.shoa.cl/n\\_cendhoc/](http://www.shoa.cl/n_cendhoc/) (Muñoz, 2020).

*Supplement.* The supplement related to this article is available online at: <https://doi.org/10.5194/bg-17-5763-2020-supplement>.

*Author contributions.* PM prepared the manuscript with contributions from all coauthors. PM, LR and LD developed the proposal and conducted field work. AM, KA and MR assisted in field work in different campaigns. All authors participated in different laboratory work and data analysis. PM, LD and KA conducted metal and radioisotope analyses. MR analyzed physical data and edited the graphs. MS helped with alpha counting on prepared samples. CM ran stable-isotope and TOC analysis. LR, CBL, PC, GS and KL assisted in specimen identification of foraminifers and diatoms. AM and IJ identified pollen and assisted with the age modeling. GV analyzed physical properties of the sediments and contributed to writing and editing the manuscript.

*Competing interests.* The authors declare that they have no conflict of interest.

*Acknowledgements.* We would like to thank the R/V *Stella Maris II* crew of Universidad Católica del Norte for their help and support during field work. We extend our acknowledgements to the laboratory assistants of the Paleoceanography Lab at Universidad de Concepción for aid in the sample analyses and to the assistants of the Oceanography Lab of Universidad Católica del Norte for aid in data analysis. We also wish to thank Olivier Bruguier of the CNRS and his lab personnel for their assistance during ICPMS analyses. We also express our gratitude to INNOVA 07CN13 IXM-150, FONDECYT 1180413 and FONDECYT 1170408. This paper was mainly funded by FONDECYT (project no. 1140851). Partial support from the COPAS Sur-Austral (CONICYT PIA PFB31 and AFB170006) and FONDAP-IDEAL centers (no. 15150003) is also acknowledged.

*Financial support.* This research has been supported by the CONICYT (grant nos. 1140851, 1180413, 1170408, PIA PFB31, AFB170006 and FONDAP-IDEAL 15150003) and the CORFO (grant no. INNOVA 07CN13 IXM-150).

*Review statement.* This paper was edited by Markus Kienast and reviewed by Matthieu Carré and two anonymous referees.

## References

- Abrantes, F.: Diatom assemblages as upwelling indicators in surface sediments off Portugal, *Mar. Geol.*, 85, 15–39, [https://doi.org/10.1016/0025-3227\(88\)90082-5](https://doi.org/10.1016/0025-3227(88)90082-5), 1988.
- Algeo, T. J. and Tribouillard, N.: Environmental analysis of paleoceanographic systems based on molybdenum-uranium covariation, *Chem. Geol.*, 268, 211–225, 2009.
- Ancapichún, S. and Garcés-Vargas, J.: Variability of the Southeast Pacific Subtropical Anticyclone and its impact on sea surface temperature off north-central Chile Variabilidad del Anticiclón Subtropical del Pacífico Sudeste y su impacto sobre la temperatura superficial del mar frente a la costa centro-norte de Chile, *Cienc. Mar.*, 41, 1–20, <https://doi.org/10.7773/cm.v41i1.2338>, 2015.
- Appleby, P. G. and Oldfield, F.: The calculation of lead-210 dates assuming a constant rate of supply of unsupported  $^{210}\text{Pb}$  to the sediment, *Catena*, 5, 1–8, [https://doi.org/10.1016/S0341-8162\(78\)80002-2](https://doi.org/10.1016/S0341-8162(78)80002-2), 1978.
- Bevington, P. and Robinson, K. (Eds.): Error analysis, in: Data Reduction and Error Analysis for the Physical Sciences, WCB/McGraw-Hill, USA, 38–52, 1992.
- Blaauw, M. and Christen, J.: Flexible paleoclimate age-depth models using an autoregressive gamma process, *Bayesian Anal.*, 6, 457–474, 2011.
- Blanco, J. L., Carr, M.-E., Thomas, A. C. and Strub, T.: Hydrographic conditions off northern Chile during the 1996–1998 La Niña and El Niño events, *J. Geophys. Res.*, 107, 3017, <https://doi.org/10.1029/2001JC001002>, 2002.
- Blott, S. J. and Pye, K.: Gradistat: A Grain Size Distribution and Statistics Package for the Analysis of Unconsolidated Sediments, *Earth Surf. Proc. Land.*, 26, 1237–1248, <https://doi.org/10.1002/esp.261>, 2001.
- Böning, P., Brumsack, H.-J., Schnetger, B., and Grunwald, M.: Trace element signatures of Chilean upwelling sediments at 36° S, *Mar. Geol.*, 259, 112–121, 2009.
- Böning, P., Shaw, T., Pahnke, K., and Brumsack, H.-J.: Nickel as indicator of fresh organic matter in upwelling sediments, *Geochim. Cosmochim. Ac.*, 162, 99–108, 2015.
- Braconnot, P., Luan, Y., Brewer, S., and Zheng, W.: Impact of Earth's orbit and freshwater fluxes on Holocene climate mean seasonal cycle and ENSO characteristics, *Clim. Dyn.*, 38, 1081–1092, <https://doi.org/10.1007/s00382-011-1029-x>, 2012.
- Calvert, S. E. and Pedersen, T. F.: Chapter Fourteen Elemental Proxies for Palaeoclimatic and Palaeoceanographic Variability in Marine Sediments: Interpretation and Application, *Dev. Mar. Geol.*, 1, 567–644, [https://doi.org/10.1016/S1572-5480\(07\)01019-6](https://doi.org/10.1016/S1572-5480(07)01019-6), 2007.
- Cardich, J., Sifeddine, A., Salvattecchi, R., Romero, D., Briceño-Zuluaga, F., Graco, M., Anculle, T., Almeida, C., and Gutiérrez, D.: Multidecadal Changes in Marine Subsurface Oxygenation Off Central Peru During the Last ca. 170 Years, *Front. Mar. Sci.*, 6, 1–16, <https://doi.org/10.3389/fmars.2019.00270>, 2019.
- Carré, M., Azzoug, M., Bentaleb, I., Chase, B. M., Fontugne, M., Jackson, D., Ledru, M.-P., Maldonado, A., Sachs, J., Schauer, A.: Mid-Holocene mean climate in the south eastern Pacific and its influence on South America, *Quat. Int.*, 253, 55–66, 2012.
- Carré, M., Sachs, J. P., Purca, S., Schauer, A. J., Braconnot, P., Falcón, R. A., Julien, M., and Lavallée, D.: Holocene history of ENSO variance and asymmetry in the eastern tropical Pacific, *Science*, 345, 1045–1048, <https://doi.org/10.1126/science.1255768>, 2014.
- Carré, M., Jackson, D., Maldonado, A., Chase, B. M., and Sachs, J. P.: Variability of  $^{14}\text{C}$  reservoir age and air–sea flux of  $\text{CO}_2$  in the Peru–Chile upwelling region during the past 12 000 years, *Quat. Res.*, 85, 87–93, 2016.
- Chaillou, G., Anschutz, P., Lavaux, G., Schäfer, J., and Blanc, G.: The distribution of Mo, U, and Cd in relation to major redox species in muddy sediments of the Bay of Biscay, *Mar. Chem.*, 80, 41–59, [https://doi.org/10.1016/S0304-4203\(02\)00097-X](https://doi.org/10.1016/S0304-4203(02)00097-X), 2002.

- Daneri, G., Dellarossa, V., Quiñones, R., Jacob, B., Montero, P., and Ulloa, O.: Primary production and community respiration in the Humboldt Current System off Chile and associated oceanic areas, *Mar. Ecol. Prog. Ser.*, 197, 41–49, <https://doi.org/10.3354/meps197041>, 2000.
- De Pol-Holz, R., Ulloa, O., Dezileau, L., Kiser, J., Lamy, F., and Hebbeln, D.: Melting of the Patagonian Ice Sheet and deglacial perturbations of the nitrogen cycle in the eastern South Pacific, *Geophys. Res. Lett.*, 33, L04704, <https://doi.org/10.1029/2005GL024477>, 2006.
- De Pol-Holz, R., Ulloa, O., Lamy, F., Dezileau, L., Sabatier, P., and Hebbeln, D.: Late Quaternary variability of sedimentary nitrogen isotopes in the eastern South Pacific Ocean, *Paleoceanography*, 22, PA2207, <https://doi.org/10.1029/2006PA001308>, 2007.
- De Pol-Holz, R., Robinson, R. S., Hebbeln, D., Sigman, D. M., and Ulloa, O.: Controls on sedimentary nitrogen isotopes along the Chile margin, *Deep-Sea Res. Pt. II*, 56, 1042–1054, <https://doi.org/10.1016/j.dsr2.2008.09.014>, 2009.
- Dezileau, L., Ulloa, O., Hebbeln, D., Lamy, F., Reyss, J. L., and Fontugne, M.: Iron control of past productivity in the coastal upwelling system off the Atacama Desert, Chile, *Paleoceanography*, 19, PA3012, <https://doi.org/10.1029/2004PA001006>, 2004.
- Díaz-Ochoa, J. A., Pantoja, S., De Lange, G. J., Lange, C. B., Sánchez, G. E., Acuña, V. R., Muñoz, P., and Vargas, G.: Oxygenation variability in Mejillones Bay, off northern Chile, during the last two centuries, *Biogeosciences*, 8, 137–146, <https://doi.org/10.5194/bg-8-137-2011>, 2011.
- Dymond, J., Suess, E., and Lyle, M.: Barium in deep-sea sediment: A geochemical proxy for paleoproductivity, *Paleoceanography*, 7, 163–181, 1992.
- Escribano, R., Daneri, G., Farías, L., Gallardo, V. A., González, H. E., Gutiérrez, D., Lange, C. B., Morales, C. E., Pizarro, O., Ulloa, O., and Braun, M.: Biological and chemical consequences of the 1997–1998 El Niño in the Chilean coastal upwelling system: A synthesis, *Deep-Sea Res. Pt. II*, 51, 2389–2411, <https://doi.org/10.1016/j.dsr2.2004.08.011>, 2004.
- Espinoza-Morriberón, D., Echevin, V., Colas, F., Tam, J., Gutierrez, D., Graco, M., Ledesma, J., and Quispelcalluari, C.: Oxygen variability during ENSO in the Tropical South Eastern Pacific, *Front. Mar. Sci.*, 5, 1–20, <https://doi.org/10.3389/fmars.2018.00526>, 2019.
- Faegri, K. and Iversen, J.: *Textbook of pollen analysis*, IV, The Blackburn Press, New Jersey, 328 pp., 1989.
- Figueroa, D. and Moffat, D.: On the influence of topography in the induction of coastal upwelling along the Chilean coast, *Geophys. Res. Lett.*, 27, 3905–3908, 2000.
- Flynn, W. W.: The determination of low levels of polonium-210 in environmental materials, *Anal. Chim. Acta*, 43, 221–227, 1968.
- Frenger, I., Bianchi, D., Sührenberg, C., Oshlies, A., Dunne, J., Deutsch, C., Galbrath, E., and Schütte, F.: Biogeochemical role of subsurface coherent eddies in the ocean: Tracer cannonballs, hypoxic storms, and microbial stewpots?, *Global Biogeochem. Cy.*, 32, 226–249, <https://doi.org/10.1002/2017GB005743>, 2018.
- Gallardo, M. A., González, A., Ramos, M., Mujica, A., Muñoz, P., Sellanes, J., and Yannicelli, B.: Reproductive patterns in demersal crustaceans from the upper boundary of the OMZ off north-central Chile, *Cont. Shelf. Res.*, 141, 26–37, 2017.
- Ganeshram, R. S., Pedersen, T. F., Calvert, S. G., McNeill, G., and Fontugne, M.: Glacial-interglacial variability in denitrification in the world's oceans: Causes and consequences, *Paleoceanography*, 15, 361–376, 2000.
- Garreaud, R., Barichivich, J., Christie, D., and Maldonado, A.: Interannual variability of the coastal fog at Fray Jorge relict forest in semiarid Chile, *J. Geophys. Res.*, 113, G04011, <https://doi.org/10.1029/2008JG000709>, 2008.
- Garreaud, R., Vuille, M., Compagnucci, R., and Marengo, J.: Present-day South American climate, *Palaeogeogr. Palaeoclimatol.*, 281, 180–195, <https://doi.org/10.1016/j.palaeo.2007.10.032>, 2009.
- Govin, A., Holzwarth, U., Heslop, D., Ford Keeling, L., Zabel, M., Mulitza, S., Collins, J. A., and Chiessi, C. M.: Distribution of major elements in Atlantic surface sediments (36° N–49° S): Imprint of terrigenous input and continental weathering, *Geochem. Geophys. Geosyst.*, 13, 1–23, <https://doi.org/10.1029/2011GC003785>, 2012.
- Grimm, E.: CONISS: a fortran 77 program for stratigraphically constrained cluster analysis by the method of incremental sum of squares, *Comput. Geosci.*, 13–35, 1987.
- Gutiérrez, D., Sifeddine, A., Reyss, J. L., Vargas, G., Velasco, F., Salvateci, R., Ferreira, V., Ortlieb, L., Field, D., Baumgartner, T., Boussafir, M., Boucher, H., Valdés, J., Marinovic, L., Soler, P., and Tapia, P.: Anoxic sediments off Central Peru record interannual to multidecadal changes of climate and upwelling ecosystem during the last two centuries, *Adv. Geosci.*, 6, 119–125, <https://doi.org/10.5194/adgeo-6-119-2006>, 2006.
- Gutiérrez, D., Enríquez, E., Purca, S., Quipuzcoa, L., Marquina, R., Flores, G., and Graco, M.: Oxygenation episodes on the continental shelf of central Peru: Remote forcing and benthic ecosystem response, *Prog. Oceanogr.*, 79, 177–189, 2008.
- Gutiérrez, D., Sifeddine, A., Field, D. B., Ortlieb, L., Vargas, G., Chávez, F. P., Velasco, F., Ferreira, V., Tapia, P., Salvateci, R., Boucher, H., Morales, M. C., Valdés, J., Reyss, J.-L., Campuano, A., Boussafir, M., Mandeng-Yogo, M., García, M., and Baumgartner, T.: Rapid reorganization in ocean biogeochemistry off Peru towards the end of the Little Ice Age, *Biogeosciences*, 6, 835–848, <https://doi.org/10.5194/bg-6-835-2009>, 2009.
- Hansen, H. P. and Koroleff, F.: Determination of nutrients, In: *Methods of Seawater Analysis*, edited by: Grasshoff, K., Kremling, K., and Ehrhardt, M., Wiley-VCH Verlag GmbH, Weinheim, Germany, 159–228, 1999.
- Haug, G. H., Hughen, K. A., Sigman, D. M., Peterson, L. C., and Röhl, U.: Southward Migration of the Intertropical Convergence Zone through the Holocene, *Science*, 293, 1304–1307, 2001.
- Hebbeln, D., Marchant, M., Freudenthal, T., and Wefer, G.: Surface distribution along the Chilean continental slope related to upwelling and productivity, *Mar. Geol.*, 164, 119–137, 2000.
- Hebbeln, D., Marchant, M., and Wefer, G.: Paleoproductivity in the southern Peru–Chile Current through the last 33 000 yr, *Mar. Geol.*, 186, 487–504, [https://doi.org/10.1016/S0025-3227\(02\)00331-6](https://doi.org/10.1016/S0025-3227(02)00331-6), 2002.
- Helly, J. and Levin, L.: Global distribution of naturally occurring marine hypoxia on continental margin, *Deep-Sea Res. Pt. I*, 51, 1159–1168, 2004.
- Heusser, C. J. and Moar, N. T.: Pollen and spores of Chile: Modern types of the pteridophyta, gymnospermae, and angiospermae, *New Zeal. J. Bot.*, 11, 389–391, <https://doi.org/10.1080/0028825X.1973.10430287>, 1973.

- Huerta-Diaz, M. A. and Morse, J. W.: Pyritization of trace metals in anoxic marine sediments, *Geochim. Cosmochim. Acta*, 56, 2681–2702, [https://doi.org/10.1016/0016-7037\(92\)90353-K](https://doi.org/10.1016/0016-7037(92)90353-K), 1992.
- Jenny, B., Valero-Garcés, B. L., Urrutia, R., Kelts, K., Veit, H., Appleby, P. G., and Geyh, M.: Moisture changes and fluctuations of the Westerlies in Mediterranean Central Chile during the last 2000 years: The Laguna Aculeo record (33°50' S), *Quatern. Int.*, 87, 3–18, 2002.
- Jenny, B., Wilhelm, D., and Valero-Garcés, B. L.: The Southern Westerlies in Central Chile: Holocene precipitation estimates based on a water balance model for Laguna Aculeo (33°50' S), *Clim. Dynam.*, 20, 269–280, <https://doi.org/10.1007/s00382-002-0267-3>, 2003.
- Kaiser, J., Schefuß, E., Lamy, F., Mohtadi, M., and Hebbeln, D.: Glacial to Holocene changes in sea surface temperature and coastal vegetation in north central Chile: high versus low latitude forcing, *Quat. Sci. Rev.*, 27, 2064–2075, 2008.
- Koutavas, A. and Joanides, S.: El Niño–Southern Oscillation extrema in the Holocene and Last Glacial Maximum, *Paleoceanography*, 27, PA4208, <https://doi.org/10.1029/2012PA002378>, 2012.
- Koutavas, A. and Lynch-Stieglitz, J.: Variability of the marine ITCZ over the Eastern Pacific during the past 30 000 years. Regional Perspective and Global Context, in: *The Hadley Circulation, Chapter 12, Advances in Global Change Research book series (Aglo, Volume 21)*, edited by: Diaz, H. F. and Bradley, R. S., Kluwer Academic Publishers, Dordrecht, the Netherlands, 347–369, 2004.
- Koutavas, A., de Menocal, P. B., Olive, G. C., and Lynch-Stieglitz, J.: Mid-Holocene El Niño–Southern Oscillation (ENSO) attenuation revealed by individual foraminifera in eastern tropical Pacific sediments, *Geology*, 34, 993–996, <https://doi.org/10.1130/G22810A.1>, 2006.
- Lamy, F., Hebbeln, D., and Wefer, G.: High-Resolution Marine Record of Climatic Change in Mid-latitude Chile during the Last 28 000 Years Based on Terrigenous Sediment Parameters, *Quat. Res.*, 51, 83–93, 1999.
- Lamy, F., Hebbeln, D., Röhl, U., and Wefer, G.: Holocene rainfall variability in southern Chile: a marine record of latitudinal shifts of the Southern Westerlies, *Earth Planet. Sc. Lett.*, 185, 369–382, 2001.
- Lamy, F., Kilian, R., Arz, H. W., Francois J.-P., Kaiser, J., Prange, M., and Steinke, T.: Holocene changes in the position and intensity of the southern westerly wind belt, *Nat. Geosci.*, 3, 695–699, 2010.
- Little, S. H., Vance, D., Walker-Brown, C., and Landing, W. M.: The oceanic mass balance of copper and zinc isotopes, investigated by analysis of their inputs, and outputs to ferromanganese oxide sediments, *Geochim. Cosmochim. Ac.*, 125, 673–693, <https://doi.org/10.1016/j.gca.2013.07.046>, 2014.
- Maldonado, A. and Rozas, E.: *Clima y Paleoambientes durante el Cuaternario Tardío en la Región de Atacama*, in: *Libro Rojo de la Flora Nativa y de los Sitios Prioritarios para su Conservación: Región de Atacama*, edited by: Squeo, F. A., Arancio, G., and Gutiérrez, J. R., Ediciones Universidad de La Serena, La Serena, Chile, 293–304, 2008.
- Maldonado, A. and Villagrán, C.: Paleoenvironmental changes in the semiarid coast of Chile (~ 32° S) during the last 6200 cal years inferred from a swamp-forest pollen record, *Quat. Res.*, 58, 130–138, 2002.
- Maldonado, A. and Villagrán, C.: Climate variability over the last 9900 cal yr BP from a swamp forest pollen record along the semiarid coast of Chile, *Quat. Res.*, 66, 246–258, <https://doi.org/10.1016/j.yqres.2006.04.003>, 2006.
- Mazzullo, J. M. and Graham, A. G. (Eds.): *Handbook for Shipboard Sedimentologists*, ODP Tech. Note, 8, 67, 1988.
- McCaffrey, R. and Thompson, J. A.: Record of the accumulation of sediment and trace metals in the Connecticut salt marsh, *Adv. Geophys.*, 22, 165–236, 1980.
- McManus, J., Berelson, W. M., Severmann, S., Poulson, R. L., Hammond, D. E., Klinkhammer, G. P., and Holm, C.: Molybdenum and uranium geochemistry in continental margin sediments: Paleoproxy potential, *Geochim. Cosmochim. Ac.*, 70, 4643–4662, 2006.
- Melo, T., Silva, N., Muñoz, P., Díaz-Naveas, J., Sellanes, J., Bravo, A., Lamilla, J., Sepúlveda, J., Vögler, R., Guerrero, Y., Bustamante, C., Alarcón, M. A., Queirolo, D., Hurtado, F., Gaete, E., Rojas, P., Montenegro, I., Escobar, R., and Zamora, V.: Caracterización del fondo marino entre la III y X Regiones, Informe Final Proyecto FIP N°2005-61, *Estud. Doc. N° 22/2007*, 287 pp., available at: [http://www.subpesca.cl/fipa/613/articles-89123\\_informe\\_final.pdf](http://www.subpesca.cl/fipa/613/articles-89123_informe_final.pdf) (last access: 5 November 2020), 2007.
- Merino-Campos, V., De Pol-Holz, R., Southon, J., Latorre, C., and Collado-Fabbri, S.: Marine radiocarbon reservoir age along the Chilean continental margin, *Radiocarbon*, 81, 1–16, <https://doi.org/10.1017/RDC.2018.81>, 2018.
- Mollier-Vogel, E., Martínez, P., Blanz, T., Robinson, R., Desprat, S., Etourneau, J., Charlier, K., and Schneider, R. R.: Mid-Holocene deepening of the Southeast Pacific oxycline, *Global Planet. Change*, 172, 365–373, 2019.
- Montecinos, A. and Aceituno, P.: Seasonality of the ENSO-Related Rainfall Variability in Central Chile and Associated Circulation Anomalies, *J. Climate*, 16, 281–296, 2003.
- Montecinos, S., Gutiérrez, J. R., López-Cortés, F., and López, D.: Climatic characteristics of the semi-arid Coquimbo Region in Chile, *J. Arid Environ.*, 126, 7–11, <https://doi.org/10.1016/j.jaridenv.2015.09.018>, 2016.
- Moraga-Opazo, J., Valle-Levinson, A., Ramos, M., and Pizarro-Koch, M.: Upwelling-Triggered near-geostrophic recirculation in an equatorward facing embayment, *Cont. Shelf Res.*, 31, 1991–1999, 2011.
- Morford, J. and Emerson, S.: The geochemistry of redox sensitive trace metals in sediments, *Geochim. Cosmochim. Ac.*, 63, 1735–1750, 1999.
- Morford, J. L., Martin, W. R., Francois, R., and Carney, C. M.: A model for uranium, rhenium and molybdenum diagenesis in marine sediments based on results from coastal locations, *Geochim. Cosmochim. Ac.*, 73, 2938–2960, 2009.
- Mortlock, R. A. and Froelich, P. N.: A simple method for the rapid determination of biogenic opal in pelagic marine sediments, *Deep-Sea Res. Pt. I*, 36, 1415–1426, [https://doi.org/10.1016/0198-0149\(89\)90092-7](https://doi.org/10.1016/0198-0149(89)90092-7), 1989.
- Muñoz, P.: Homepage, National Hydrographic and Oceanographic Data Center of Chile – CENDHOC, available at: [http://www.shoa.cl/n\\_cendhoc/](http://www.shoa.cl/n_cendhoc/), last access: 5 November 2020.

- Muñoz, P., Dezileau, L., Lange, C., Cárdenas, L., Sellanes, J., Salamanca, M., and Maldonado A.: Evaluation of sediment trace metal records as paleoproductivity and paleoxygenation proxies in the upwelling center off Concepción, Chile (36° S), *Prog. Oceanogr.*, 92–95, 66–80, <https://doi.org/10.1016/j.pocean.2011.07.010>, 2012.
- Nameroff, T., Balistrieri, L., and Murray, W.: Suboxic trace metals geochemistry in the eastern tropical North Pacific, *Geochim Cosmochim. Acta.*, 66, 1139–1158, 2002.
- Niemeyer, H. F.: Hoyas Hidrográficas de Chile, Cuarta Región, Centro de Información de Recursos Hídricos, Dirección General de Aguas, available at: <https://snia.mop.gob.cl/sad/CUH2886v4.pdf> (last access: 5 November 2020), 4, 258–297, 2018.
- Ohnemus, D. C. and Lam, P. J.: Cycling of lithogenic marine particles in the US GEOTRACES North Atlantic transect, *Deep-Sea Research Part II: Topical Studies in Oceanography*, 116, 283–302, <https://doi.org/10.1016/j.dsr2.2014.11.019>, 2015.
- Ortega, C., Vargas, G., Rutllant, J. A., Jackson, D., and Méndez, C.: Major hydrological regime change along the semiarid western coast of South America during the early Holocene, *Quat. Res.*, 78, 513–527, 2012.
- Ortega, C., Vargas, G., Rojas, M., Rutllant, J. A., Muñoz, P., Lange, C. B., Pantoja, S., Dezileau, L., and Ortlieb, L.: Extreme ENSO-driven torrential rainfalls at the southern edge of the Atacama Desert during the late Holocene and their projection into the 21st century, *Global Planet. Change*, 175, 226–237, <https://doi.org/10.1016/j.gloplacha.2019.02.011>, 2019.
- Paytan, A.: Ocean paleoproductivity, *Encyclopedia of Paleoclimatology and Ancient Environments*, in: *Encyclopedia of Earth Science Series*, edited by: Gornitz, V., Springer, Dordrecht, the Netherlands, [https://doi.org/10.1007/978-1-4020-4411-3\\_158](https://doi.org/10.1007/978-1-4020-4411-3_158), 2009.
- Peacock, C. L. and Sherman, D. M.: Copper(II) sorption onto goethite, hematite and lepidocrocite: a surface complexation model based on ab initio molecular geometries and EXAFS spectroscopy, *Geochim. Cosmochim. Acta.*, 68, 2623–2637, 2004.
- Pizarro, O., Hormazabal, S., Gonzalez, A., and Yañez, E.: Variabilidad del viento, nivel del mar y temperatura en la costa norte de Chile, *Invest. Mar.*, 22, 85–101, 1994.
- Pizarro, O., Shaffer, G., Dewitte, B., and Ramos, M.: Dynamics of seasonal and interannual variability of the Peru-Chile Undercurrent, *Geophys. Res. Lett.*, 29, 28–31, <https://doi.org/10.1029/2002GL014790>, 2002.
- Pizarro-Koch, M., Pizarro, O., Dewitte, B., Montes, I., Ramos, M., Paulmier, A., and Garçon, V.: Seasonal variability of the southern tip of the Oxygen Minimum Zone in the eastern South Pacific (30°–38° S): A modeling study, *J. Geophys. Res.-Oceans*, 124, 8574–8604, <https://doi.org/10.1029/2019JC015201>, 2019.
- Quintana, J. M. and Aceituno, P.: Changes in the rainfall regime along the extratropical west coast of South America (Chile): 30–43° S, *Atmosfera*, 25, 1–22, 2012.
- Rahn, D. A. and Garreaud, R. A.: A synoptic climatology of the near-surface wind along the west coast of South America, *Int. J. Climatol.*, 34, 780–792, <https://doi.org/10.1002/joc.3724>, 2013.
- Ramos, M., Pizarro, O., Bravo, L., and Dewitte, B.: Seasonal variability of the permanent thermocline off northern Chile, *Geophys. Res. Lett.*, 33, L09608, <https://doi.org/10.1029/2006GL025882>, 2006.
- Ramos, M., Dewitte, B., Pizarro, O., and Garric, G.: Vertical propagation of extratropical Rossby waves during the 1997–1998 El Niño off the west coast of South America in a medium-resolution OGCM simulation, *J. Geophys. Res.*, 113, C08041, <https://doi.org/10.1029/2007JC004681>, 2008.
- Reimer, P. J., Bard, E., Bayliss, A., Beck, J. W., Blackwell, P. G., Ramsey, C. B., Buck, C. E., Cheng, H., Edwards, R. L., Friedrich, M., Grootes, P. M., Guilderson, T. P., Haffidason, H., Hajdas, I., Hatté, C., Heaton, T. J., Hoffmann, D. L., Hogg, A. G., Hughen, K. A., Kaiser, K. F., Kromer, B., Manning, S. W., Niu, M., Reimer, R. W., Richards, D. A., Scott, E. M., Southon, J. R., Staff, R. A., Turney, C. S. M., and van der Plicht, J.: IntCal13 and Marine13 Radiocarbon Age Calibration Curves 0–50 000 Years cal BP, *Radiocarbon*, 55, 1869–1887, [https://doi.org/10.2458/azu\\_js\\_rc.55.16947](https://doi.org/10.2458/azu_js_rc.55.16947), 2013.
- Rein, B., Lückge, A., Reinhardt, L., Sirocko, F., Wolf, A., and Dullo, W.-C.: El Niño variability off Peru during the last 20 000 years, *Paleoceanography*, 20, PA4003, <https://doi.org/10.1029/2004PA001099>, 2005.
- Rutllant, J. and Fuenzalida, H.: Synoptic aspects of the central Chile Rainfall variability associated with the southern oscillation, *Int. J. Climatol.*, 11, 63–76, 1991.
- Sabatier, P., Dezileau, L., Blanchemanche, P., Siani, G., Condomines, M., Bentaleb, I., and Piquès, G.: Holocene variations of radiocarbon reservoir ages in a mediterranean lagoonal system, *Radiocarbon*, 52, 91–102, <https://doi.org/10.1017/S0033822200045057>, 2010.
- Sadler, P. M.: The Influence of Hiatuses on Sediment Accumulation Rates, *GeoResearch Forum*, 5, 15–40, 1999.
- Saito, C., Noriki, S., and Tsunogai, S.: Particulate flux of Ai, a component of land origin, in the western North Pacific, *Deep-Sea Res.*, 39, 1315–1327, 1992.
- Salvatteci, R., Gutiérrez, D., Sifedine, A., Ortlieb, L., Druffel, E., Boussafir, M., and Schneider, R.: Centennial to millennial-scale changes in oxygenation and productivity in the Eastern Tropical South Pacific during the last 25 000 years, *Quat. Sci. Rev.*, 131, 102–117, 2016.
- Salvatteci, R., Schneider, R. R., Blanz, T., and Mollier-Vogel, E.: Deglacial to Holocene ocean temperatures in the Humboldt Current System as indicated by alkenone paleothermometry, *Geophys. Res. Lett.*, 46, 281–292, <https://doi.org/10.1029/2018GL080634>, 2019.
- Sandweiss, D. H., Maasch, K. A., Andrus, C., Fred, T., Reitz, E. J., Richardson III, J. B., Riedinger-Whitmore, M., and Rollins, H. B.: Mid-Holocene climate and culture change in coastal Peru, Chapter 2, in: *Climate Change and Cultural Dynamics: A Global Perspective on Mid-Holocene Transitions*, edited by: Anderson, D. G., Maasch, K. A., and Sandweiss, D. H., Elsevier Academic Press, Burlington, MA, USA, <https://doi.org/10.1016/B978-012088390-5.50007-8>, 25–50, 2007.
- Scholz, F., Hensen, C., Noffke, A., Rohde, A., Liebetrau, V., and Wallmann, K.: Early diagenesis of redox-sensitive trace metals in the Peru upwelling area – response to ENSO-related oxygen fluctuations in the water column, *Geochim. Cosmochim. Acta.*, 75, 7257–7276, 2011.
- Schrader, H. J. and Gersonde, R.: Diatoms and silicoflagellates, *Utrecht Micropaleontol. Bull.*, 17, 129–176, 1978.
- Sellanes, J., Quiroga, E., Neira, C., and Gutiérrez, D.: Changes of macrobenthos composition under different ENSO cycle condi-

- tions on the continental shelf off central Chile, *Cont. Shelf Res.*, 27, 1002–1016, 2007.
- Shaffer, G., Pizarro, O., Djurfeldt, L., Salinas, S., and Rutllant, J.: Circulation and low-frequency variability near the Chilean coast: Remotely forced fluctuations during the 1991–92 El Niño, *J. Phys. Oceanogr.*, 27, 217–235, 1997.
- Shaffer, G., Hormazabal, S., Pizarro, O., and Salinas, S.: Seasonal and interannual variability of currents and temperature over the slope of central Chile, *J. Geophys. Res.*, 104, 29951–29961, 1999.
- Siebert, C., Nägler, T. F., von Blackenburg, F., and Kramers, J. D.: Molybdenum isotope records as a potential new proxy for paleoceanography, *Earth Planet. Sc. Lett.*, 6643, 1–13, 2003.
- Sigman, D. M., Karsh, K. L., and Casciotti, K. L.: Ocean process tracers: nitrogen isotopes in the ocean, *Encyclopedia of ocean science*, 2nd edn., Elsevier, Amsterdam, 2009.
- Sundby, B., Martinez, P., and Gobeil, C.: Comparative geochemistry of cadmium, rhenium, uranium, and molybdenum in continental margin sediments, *Geochim. Cosmochim. Ac.*, 68, 2485–2493, 2004.
- Sweeney, R. E. and Kaplan I. R.: Natural abundances of  $^{15}\text{N}$  as a source indicator of nearshore marine sedimentary and dissolved nitrogen, *Mar. Chem.*, 9, 81–94, 1980.
- Torres, M. E., Brumsack, H. J., Bohrmann, G., and Emeis, K. C.: Barite front in continental margin sediments: a new look at barium remobilization in the zone of sulfate reduction and formation of heavy barites in diagenetic fronts, *Chem. Geol.*, 127, 125–139, 1996.
- Torres, R. and Ampuero, P.: Strong  $\text{CO}_2$  outgassing from high nutrient low chlorophyll coastal waters off central Chile ( $30^\circ\text{S}$ ): The role of dissolved iron, *Estuar. Coast. Shelf Sci.*, 83, 126–132, <https://doi.org/10.1016/j.ecss.2009.02.030>, 2009.
- Toth, L. T., Aronson, R. B., Vollmer, S. V., Hobbs, J. W., Urrego, D. H., Cheng, H., Enochs, I. C., Combosch, D. J., van Woesik, R., and Macintyre, J. G.: ENSO Drove 2500-Year Collapse of Eastern Pacific Coral Reefs, *Science*, 337, 81–84, <https://doi.org/10.1126/science.1221168>, 2012.
- Tribovillard, N., Riboulleau, A., Lyons, T., and Baudin, F.: Enhanced trapping of molybdenum by sulfurized organic matter of marine origin as recorded by various Mesozoic formations, *Chem. Geol.*, 213, 385–401, 2004.
- Tribovillard, N., Algeo, T. J., Lyons, T., and Riboulleau, A.: Trace metals as paleoredox and paleoproductivity proxies: an update, *Chem. Geol.*, 232, 12–32, 2006.
- Ulloa, O., Escribano, R., Hormazabal, S., Quiñones, R. A., González, R., and Ramos, M.: Evolution and biological effects of the 1997–98 El Niño in the upwelling ecosystem off northern Chile, *Geophys. Res. Lett.*, 28, 1591–1594, 2001.
- Ulloa, O., Canfield, D. E., DeLong, E. F., Letelier, R. L., and Stewart, F. J.: Microbial oceanography of anoxic oxygen minimum zones, *P. Natl. Acad. Sci. USA*, 109, 15996–16003, <https://doi.org/10.1073/pnas.1205009109>, 2012.
- Valle-Levinson, A. and Moraga-Opazo, J.: Observations of bipolar residual circulation in two equatorward-facing semiarid bays, *Cont. Shelf Res.*, 26, 179–193, <https://doi.org/10.1016/j.csr.2005.10.002>, 2006.
- Valle-Levinson, A., Moraga, J., Olivares, J., and Blanco, J. L.: Tidal and residual circulation in a semi-arid bay: Coquimbo Bay, Chile, *Cont. Shelf Res.*, 20, 2009–2018, 2000.
- Van der Weijden, C.: Pitfalls of normalization of marine geochemical data using a common divisor, *Mar. Geol.*, 184, 167–187, 2002.
- Vance, D., Archer, C., Bermin, J., Perkins, J., Statham, P. J., Lohan, M. C., Ellwood, M. J., and Mills, R. A.: The copper isotope geochemistry of rivers and the oceans, *Earth Planet. Sc. Lett.*, 274, 204–213, 2008.
- Vargas, G., Ortlieb, L., Pichon, J. J., Bertaux, J., and Pujos, M.: Sedimentary facies and high resolution primary production inferences from laminated diatomaceous sediments off northern Chile ( $23^\circ\text{S}$ ), *Mar. Geol.*, 211, 79–99, <https://doi.org/10.1016/j.margeo.2004.05.032>, 2004.
- Vargas, G., Rutllant, J., and Ortlieb, L.: ENSO tropical–extratropical climate teleconnections and mechanisms for Holocene debris flows along the hyperarid coast of western South America ( $17^\circ$ – $24^\circ\text{S}$ ), *Earth Planet. Sc. Lett.*, 249, 467–483, 2006.
- Veit, H.: Southern Westerlies during the Holocene deduced from geomorphological and pedological studies in the Norte Chico, Northern Chile ( $27$ – $33^\circ\text{S}$ ), *Palaeogeogr. Palaeoclimatol.*, 123, 107–119, 1996.
- Vergara, O., Dewitte, B., Montes, I., Garçon, V., Ramos, M., Paulmier, A., and Pizarro, O.: Seasonal variability of the oxygen minimum zone off Peru in a high-resolution regional coupled model, *Biogeosciences*, 13, 4389–4410, <https://doi.org/10.5194/bg-13-4389-2016>, 2016.
- Xu, G., Liu, J., Pei, S., Kong, X., Hu, G., and Gao, M.: Source identification of aluminum in surface sediments of the Yellow Sea off the Shandong Peninsula, *Acta Oceanol. Sin.*, 34, 147–153, <https://doi.org/10.1007/s13131-015-0766-9>, 2015.
- Yang, S. and Oh, J.-H.: Effects of modes of climate variability on wave power during boreal summer in the western North Pacific, *Sci. Rep.*, 10, 5187, 1–10, <https://doi.org/10.1038/s41598-020-62138-0>, 2020.
- Zheng, Y., Anderson, R. F., van Geen, A., and Fleisheir, M. Q.: Preservation of non-lithogenic particulate uranium in marine sediments, *Geochim. Cosmochim. Ac.*, 66, 3085–3092, 2002.